universität wien

MASTERARBEIT / MASTER'S THESIS

Titel der Masterarbeit / Title of the Master's Thesis

„Computational modelling of cellular senescence in liver tissue“

verfasst von / submitted by

Helene Kaufmann, BSc

angestrebter akademischer Grad / in partial fulfilment of the requirements for the degree of

Master of Science (MSc)

Wien, 2024 / Vienna 2024

Studienkennzahl lt. Studienblatt / degree programme code as it appears on the student record sheet:	UA 066 606
Studienrichtung lt. Studienblatt / degree programme as it appears on the student record sheet:	Masterstudium Drug Discovery and Development
Betreut von / Supervisor:	Assoc.-Prof. Dr. Joost Beltman

Acknowledgments

To begin with, I would like to thank my daily supervisor Elsje Burgers for the time she dedicated to giving me advice, and the productive, yet enjoyable meetings we had together. Additionally, I want to express my thanks to my supervisor Joost Beltman, who made it possible for me to work on this exciting project and offered his precious advice whenever I needed it.

I am grateful for the opportunity to have become a part of the Beltman group. My office mates Levi Winkelman, Filippo di Tillio, and Hanneke Leegwater treated me as a natural member from day one. This led to inspiring conversations and new scientific insights, as well as a good personal connection that supported me throughout the project.

My biggest thanks go to my parents who supported me unconditionally throughout my life and did not hesitate for a moment to support this project abroad. I am grateful for my friends who have been a constant source of motivation, some even from afar. Last but not least I want to thank my partner, a great mentor who never stops believing in me.

PREFACE

Public summary

Accumulation of senescent cells in aging tissue is involved in many age-related diseases. Due to the heterogeneity of these cells, the mechanisms in the aging liver have not yet been sufficiently explored to enable the development of effective treatment options. In this study, two different mathematical models were established to allow the investigation of the mechanisms at play.

Keywords

Cellular senescence, Liver, Single-cell transcriptomics, Ordinary Differential Equation model, Boolean model

Abstract

Cellular senescence is a state characterized by irreversible cell cycle arrest, the inflammatory senescence-associated secretory phenotype (SASP), altered metabolism, and other cellular changes. On the one hand, entering this state can work as a protective mechanism, but on the other hand, these cells have been shown to accumulate with age and contribute to age-related diseases. A better understanding of the mechanisms involved in the accumulation of these cells is valuable for finding unique traits to target these cells. In this work, two distinct mathematical modeling approaches were used to investigate these mechanisms in a healthy aging liver. In single-cell transcriptomics data of mice, we were able to find p38MAPK and NF-κB mediated SASP factors to be expressed in more cells during aging and were able to quantify the increase in senescence with a score. This data was used in an ordinary differential equation model. The model that described the data best, indicated a cell cycle arrest-dependent increase in senescence that is independent of the SASP. However, it was not yet possible to show that this model is the optimal solution for this data. Additionally, we were able to capture the interaction of senescent cells with the immune system in a literature-based Boolean model. In four different scenarios, which include the senescent and healthy state of the tissue, as well as the development of two resistance mechanisms, the model matched the expected behavior. We were able to highlight challenges in the approach and provided models that are a good foundation for further modeling efforts.

KURZFASSUNG

Zelluläre Seneszenz ist ein Zustand, der durch einen irreversiblen Zellzyklus-Arrest, ein pro-inflammatorisches Sekretom, genannt SASP, einen veränderten Stoffwechsel und andere zelluläre Veränderungen gekennzeichnet ist. Einerseits kann der Eintritt in diesen Zustand als Schutzmechanismus wirken, andererseits hat sich gezeigt, dass sich diese Zellen mit dem Alter ansammeln und zu altersbedingten Krankheiten beitragen. Ein besseres Verständnis der Mechanismen, die an der Anhäufung dieser Zellen beteiligt sind, ist wichtig, um Eigenschaften zu finden, die es erlauben diese Zellen gezielt zu behandeln. In dieser Arbeit wurden zwei verschiedene mathematische Modellierungsansätze verwendet, um diese Mechanismen in einer gesunden alternden Leber zu untersuchen. In single-cell transcriptomics Daten konnten wir feststellen, dass die Expression von p38MAPK und von NF-κB verursachtem SASP im Laufe des Alterungsprozesses vermehrt in Zellen gemessen wurde, und die Akkumulation von zellulärer Seneszenz mit einem Score quantifizieren. Mit diesen Daten wurde ein ordinary differential equation model erstellt. Der beste Fit des Modells wies darauf hin, dass die Zunahme der Seneszenz abhängig vom Zellzyklusarrest ist, nicht jedoch vom SASP. Allerdings konnte noch nicht gezeigt werden, dass dieses Modell die optimale Lösung für diese Daten darstellt. Des Weiteren konnten wir die Interaktion von seneszenten Zellen mit dem Immunsystem in einem literaturbasierten Boolean model erfassen. In vier verschiedenen Szenarien, die den seneszenten und gesunden Zustand des Gewebes sowie die Entwicklung von zwei Resistenzmechanismen umfassen, entsprach das Modell dem erwarteten Verhalten. Wir konnten die Herausforderungen der Ansätze aufzeigen und Modelle erstellen, die als gute Grundlage für weitere Modellierungsversuche dienen können.

CONTENTS

Acknowledgments III
Preface V
Public summary V
Keywords V
Abstract VII
Kurzfassung IX
Contents XI
Introduction 1
Methods 4
1. The data set 4
2. Pathway analysis 4
3. Scoring of senescent cells 5
4. The ODE model 5
5. Boolean model 7
6. Usage of AI models 7
7. Code availability 7
Results 8
Cell cycle arrest and inflammatory pathways are upregulated in senescence 8
Elimination of senescent cells can be aggravated by multiple mechanisms 10
The aging process in the liver was captured in a single cell resolution 11
The P38MAPK and NF-κB pathways are increasingly expressed over time 13
Dynamic inflammatory proteins are likely regulated by NF-κB 16
Immune cell recruitment could not be not observed in the data 17
Overlap of known senescent markers is restricted to advanced age 18
Senepy reveals dynamics of senescence 20
Cell cycle arrest and inflammation pathways show distinct dynamics 22
Increasing rate of p38MAPK induction is necessary to describe the biological interactions 24
The Boolean model captures simple interactions between senescent cells and the immune system 28
Discussion 32
References 37
Appendix 45
Pathway maps 45

Protein to gene conversion 48
Pathway gene dynamics 49
ODE fitting results and model equations 51
Boolean model rules and example 55

1

Introduction

Throughout the past 30 years, the importance of the field of cellular senescence has become increasingly evident and has inspired researchers to dedicate their efforts to this cause.[1] The term cellular senescence was coined to describe a state where cells undergo mostly irreversible cell cycle arrest, display an inflammatory secretory phenotype, and are subject to macromolecular damage and altered metabolism, as well as other changes.[2] As a result of the onset of the senescence-associated secretory phenotype (SASP), immune cells that eliminate the non-dividing senescent cells are recruited.[3] Cellular senescence can be seen as a protective mechanism of the body to prevent the proliferation of damaged cells, which can be conceptually compared to apoptosis.[4] This protection mechanism is especially important at an advanced age when cellular damage increases and entering the senescent state can stop the cell from causing further harm, for example by turning into a cancer cell.[4] However, the importance of this program is not limited to aging but is also evident in development and tissue repair[5–7].

Even though cellular senescence was first discovered as a phenomenon resulting from the shortening of telomeres of aged cells[8], later many non-age related causes for the onset of the program were discovered. Among the most important ones are DNA damage response (DDR), oxidative stress, oncogene activation, and epigenome changes.[9–11] Once senescent, the cell cycle arrest is generally irreversible, but it has been shown that by blockade of AMPK-TAB1–dependent activation of p38 in senescent T cells, the defective proliferation was resolved.[12] This indicates that there may be certain influences which are not yet understood that can reverse the process. Nonetheless, experts claim that under physiological conditions, after more than five days in the senescent state, re-entry of a proliferative state is unlikely.[13–15]

In young individuals, the senescent cells are readily eliminated by the immune system, so the inflammatory signals do not persist.[3,16] However, this rate of clearing decreases as the organism ages, leading to the accumulation of senescent cells in tissues and organs. This accumulation can cause age-related diseases, chronic inflammation, and cancer.[3,17–20] Why this clearance is increasingly impaired over time, is not yet fully understood. One primary cause might be the aging of the immune system, another the impairment of immune surveillance by

the accumulation of senescent cells themselves.[21] The first theory is supported by the observation that impaired DNA repair in hematopoietic cells led not only to immune cells becoming senescent but also to the accumulation of senescent cells in non-lymphoid organs.[22]. The latter theory was developed because senescent cells expressing surface molecules such as types of MHC I or proteins like PD-L1 showed resistance against clearance by immune cells.[23,24]

Accumulation of senescent cells is not only thought to contribute to diseases but it is even thought to play a causal role in some features of general organismal ageing.[4,25–28] Indeed, efforts to eliminate senescent cells *in vivo*, resulted in the extension of the healthy life span and relief of aging-related dysfunctions.[3,29] This study highlighted the impact, that successful treatments could have. So far, drug discovery efforts have been focused on two main approaches: specifically eliminating senescent cells, and inhibiting the SASP.[30] Counteracting the SASP can be achieved by neutralizing SASP components, or by targeting known SASP drivers, for example, nuclear factor kappa-light-chain-enhancer of activated B cells (NF-κB).[30,31] For example, compounds known to prolong life like rapamycin have shown some efficacy in reducing the SASP.[30,32,33] However, this strategy is not without issues, as most of these compounds have shown toxicities after long-term usage, and all effects of the SASP are inhibited, including the positive ones.[30] To selectively target and eliminate senescent cells with senolytic drugs, a common trait needs to be found. For example their resistance to apoptosis was utilized by inhibiting the Bcl-2 family of anti-apoptotic proteins.[30] Other exploited mechanisms are the exclusion of p53 from the nucleus[30,31], and CAR T-cell therapy specific to cell surface molecules[34]. Limitations of these treatments are the lack of specificity to harmful senescent cells and that only subsets of senescent cells are successfully targeted.[30] Therefore, the heterogeneity of the cells and thus the lack of universal features are described as limiting for the efficient application of therapies.[3,35]

This heterogeneity is apparent in studies where different stressors are applied on the same cell line, which resulted in different patterns of senescence marker expression. The pattern is not specific to the stressor, as the same cell line treated with the stressor, showed again a different pattern.[36,37] Since even *in vitro* studies yield such high heterogeneity, it is not surprising that the heterogenous senescence pattern *in vivo*[38] is even more pronounced.

To investigate the markers and pathways that are responsible for the accumulation of senescent cells during the aging process, *in vivo* data collected throughout the life span is required. Previous studies that attempted to capture these interactions were limited by the low number of time points obtained for proteomics data and only investigated senescence as a response to acute stressors[39], not aging. To tackle those shortcomings, we used single-cell

transcriptomics data of the liver of mice throughout their lives to examine the interactions. Since the liver is constantly exposed to antigens from the alimentary tract, there is a unique balance between immune tolerance and combating local injury and inflammation.[40] Shedding light on how senescent cells accumulate and interact with the immune system in that special environment, can provide a valuable foundation for drug discovery efforts.

After we identified the most important senescence-related pathways from the literature, we analyzed the genes of these pathways in the single-cell transcriptomics data for changes in the percentage of cells expressing the genes over time. Among the pathways where the increase was the most clearly visible, were the p38MAPK pathway leading to cell cycle arrest and the inflammatory pathway NF-κB which is responsible for the regulation of many inflammatory factors that are part of the SASP. Since senescence is not governed by a single pathway, but by many, it is challenging to measure the change in senescent cells in transcriptomics data. Recently, a package called Senepy[41] has been developed, that allowed for the calculation of a senescence score to indicate if a cell is likely senescent or not.

To model the interactions of cell cycle arrest, SASP, and the rise in senescent cells with age, an ordinary differential equation (ODE) approach was taken. In this model, the three variables were described with ODEs that mirror their anticipated interactions. After building eight different versions, the model best describing the data was obtained when the rise of senescence was dependent on cell cycle arrest, but not on the SASP. In this model, the rate of induction of cell cycle arrest increased with age. However, it could not be shown that this is the only possible solution for the data.

On the microenvironmental level, the interaction of the immune system with senescent cells could be described with a small-scale literature-based Boolean model. Boolean models which can simulate nodes that interact with each other following defined rules, can reveal the dynamics of a system, and how it can be influenced. These insights can be valuable to estimate the impact of possible targets, especially considering many different biological conditions.[42] In a simulation of the microenvironment of a senescent cell, including T lymphocytes, pro-inflammatory and anti-inflammatory macrophages, resistant senescent cells, and anti-inflammatory SASP, four different scenarios have been simulated. These simulations were able to portray the influence of the SASP composition and the impact of resistant senescent cells. Further extensions of the model will allow even more valuable insights into the interactions in the microenvironment.

2

Methods

1. The data set

The dataset used for this work, known as the Tabula Muris Senis, includes single-cell transcriptomic data of the liver in C57BL/6JN mice. This dataset spans observations from mice aged 1 month to 30 months. The first time point would be equivalent to the childhood stage in humans.[43] Since cellular senescence plays a role in developmental processes[44], the 1-month time point was excluded from all analyses in this work. The liver data obtained by the microfluidic droplet method was downloaded in .h5ad format from Cellxgene[45]. The authors already conducted pre-processing steps including the removal of low-quality data points, normalization, scaling, clustering with the Louvain method, and cell type annotation. A more detailed description can be found in the original work[46].

2. Pathway analysis

To find the pathways in the dataset that were expressed in more cells over time, relevant pathways from literature were selected. The dynamics of the genes required for the pathways were visualized. For this analysis only a selection of cell types was used: Hepatocytes, Kupffer cells and endothelial cells. For the gene dynamics visualization, the percentage of cells expressing a selected gene at each time point was calculated.

The KEGG database[47] for pathways was used as a source of information on proteins that are part of the pathways described as relevant in the literature. Since the KEGG database includes human proteins but the data set mouse RNA, the NIH gene database[48] was used to associate the protein in the pathway map with the respective mouse RNA (Supplementary table 1). The maps used from KEGG were entitled Cellular senescence, NF-kappa B signaling pathway, JAK-STAT signaling pathway, TNF signaling pathway, PD-L1 expression and PD-1 checkpoint pathway, and Cytokine-cytokine receptor interaction. All analyzed pathways and proteins of these maps can be found in the appendix (Supplementary figure 1-5).

For the DGE analysis, 30-month-old mice were compared to 3-month-old mice, and the differentially expressed genes were filtered for those that were included in a list of human inflammatory proteins[49]. To investigate the transcription factors targeting the inflammatory proteins, we used DoRothEA[50] and Transcription Factor Target Gene Database[51].

3. Scoring of senescent cells

To quantify senescence in the data set, we used the Senepy package built by Sanborn *et al.*[41] It enables the user to get a senescence score for each cell in a single-cell dataset based on cell type-specific gene correlation hubs. The cell hubs were obtained by a multi-step analysis. First, genes that were expressed in less than 1 % of the cells in early time points and in 1-20 % of the late time points were selected and underwent a correlation analysis. Genes and interactions with a high correlation were portrayed by graph networks and grouped with the Louvain algorithm. After discarding genes with low connectivity to other genes, there were two gene hubs for each, hepatocytes, endothelial cells, and Kupffer cells left. Since no hubs for other cell types are included in the package, all other cell types were excluded from the further analysis. To score the dataset, each cell type was processed separately. The Senepy scoring function separates all genes in the data set into 25 bins, according to their mean expression. From each bin containing a gene from the signature hub, there are 50 other genes chosen at random. Then the mean of the control genes in each cell is subtracted from the hub gene expression which yields the Senepy score. Since there are two hubs available for each cell type, the cells were first scored with both hubs separately and thereafter, the higher score was chosen.

The second approach to quantify senescent cells was based on a panel of markers that were derived from literature and the data was investigated for cells expressing the genes in the panel.

4. The ODE model

To fit the parameters in the ODEs to the data, a script from Heldring *et al*.[52] was used and adjusted as required. The script was originally intended for modeling drug induced stress response, using data with multiple doses and replicates. After testing both variants, it proved easier to adjust the data format to the script than the script to a new data format. Hence, data columns for the dose level were added, and empty replicates were created for time points with less than three replicates.

The script is based on the least squares method, using 'least_squares' function from Scipy[53]. It minimizes the cost function *F(x)* (Equation 1) which is dependent on the squared residuals. The residuals are the difference between the estimated data point and the mean of the real data point. The vector containing *m* residuals is computed by the residuals function $f_i(x)$. In the script from Heldring *et al.* the residuals are divided by the standard deviation (sd) of the time point. As a result, for time points with a high sd, the residual value is decreased which causes the point to have less impact on the cost and therefore on the fitting outcome. However, in the data set there were two time points with no replicates, which would result in an sd of 0. In the algorithm, the residuals of these two points were not divided by any number, which is equivalent to dividing by 1. After observing that these points were not sufficiently taken into account in the fitting process, the divisor was lowered to 0.6 instead of 1. This number was the result of fitting the same model using different divisors starting from the original value of 1 and then decreasing. The sds of the variables at the first time point were between 0.18 and 4.0, which places the chosen value among the lower ones. This resulted in the best weight balance for fitting between the data points with and without sd.

Equation 1. Cost function.

$$F(x) = 0.5 * \sum f_i(x)^2, i = 0, \ldots, m - 1$$

In the original script for parameter fitting, the mean is calculated from all replicates, which would attribute the same importance to all mice. Since in this dataset, the amount of cells per sample varies greatly, a weighted average was used instead. These weights for every data point were calculated based on the total number of cells obtained from that mouse (Equation 2). If the data points connected to one variable were in a lower range than the data from other variables, less importance was given to the former. Hence, the data points associated with each variable were scaled to the highest time point so their dynamics would be equally important.

Equation 2. Weighted average.

$$\bar{X} = \frac{\sum x_i * w_i}{\sum w_i}$$

The terms used in the equations were limited to linear terms. For establishing each equation, some general rules were followed. There was always a basal induction (basal in the sense that the inducer is not specified in the model) and a basal degradation. The initial value chosen for

the estimation of each equation was the weighted mean of the first time point. The script includes the option to set a prior that defines a starting value for a parameter, which was used for fitting the final version of model E. We also used the option to fit parameters for offset and scaling for every variable. The final cost of each set of parameters was used as an indicator for a good fit when evaluating the results. Although a low cost value did not necessarily provide a better match of the dynamics than a slightly higher cost function. As the goal was to get a good qualitative not a quantitative fit, at least ten out of 200 sets with the lowest cost were analyzed for a good dynamical fit.

5. Boolean model

To establish the Boolean model, we created a network of nodes that are connected by rules based on findings from the literature. We used the BoolNet[54] package that provides the necessary functions to iteratively apply the rules to the current state. We introduced an additional function that keeps nodes in an inactive state until a certain number of iterations have been completed. The transition into an active state thereafter has to be induced by the other nodes. Additionally, we added a function that kept the senescent cell in an inactive state once the cell had been deactivated. The simulations were averaged over 200 runs and each run included 41 iterations.

6. Usage of AI models

For this work, ChatGPT 3.5 and 4.0 was used for spell-checking the written report and for syntax control and simplification of the code. In addition, Grammarly was used for spell-checking and grammar corrections. Microsoft Copilot was used to look for relevant websites.

7. Code availability

The code that was written for the Boolean model and the ODE model is available on Github (https://github.com/KaufmannH/liver_senescence). It also includes the adapted scripts from Heldiring *et al.*[52] and the scripts used to create the graphs for this work.

3

RESULTS

CELL CYCLE ARREST AND INFLAMMATORY PATHWAYS ARE UPREGULATED IN SENESCENCE

One of the pronounced features of senescent cells is the permanent cell cycle arrest. Two protein families that are important to establish the arrest are p53 and pRB.[2] The transcription factor p53 is activated as a result of p38MAPK or ATM pathway induction by ROS or DNA damage (Figure 1A). The other relevant axis that can induce cell cycle arrest is the phosphorylation of the transcriptional repressor protein pRB after the activation of the cyclin-dependent kinase (CDK) inhibitor p16.[55] An important target gene of p53 is p21, which is a CDK inhibitor, like p16. If the CDK/cyclin complex is bound by p21 and p16, it cannot phosphorylate the transcriptional repressor pRB. In the hypophosphorylated state, pRB remains bound to the E2F transcription factor which is needed in a free state for DNA replication.[2,56] Despite the established role of cell cycle arrest in the senescence phenotype, Gorgoulis *et al*.[2] believe that proliferation arrest is not always a necessary outcome of senescence, as even post-mitotic cells have been shown to acquire senescence-like features. Moreover, the cell cycle arrest in senescent cells has been reversed *in vitro*. However, these cells did not return to their initial state, instead, they acquired genomic changes.[57] A study investigating the mechanisms of the reversal processes in senescent HEK cells found that depletion of p21 via RNAi led to reversal of the arrest. The same was observed after depletion of p16, which suggests that both CDKs are needed for irreversible cell cycle arrest.[58] However, it cannot be assumed that both markers are universally expressed in all senescent cells. For example, human fibroblasts *in vitro* showed either strong expression of p21 or p16, with only a small fraction of cells being positive for both.[59] Those contradictory findings highlight again the heterogeneity of the senescent state.

In addition to cell cycle arrest, an important hallmark of senescence is the SASP, which is characterized by the excretion of inflammatory proteins. The transcription of these proteins can be regulated by many transcription factors, but the most important ones are NF-κB [60], GATA4[61] and CCAAT/enhancer binding protein beta (C/EBPb)[62]. Nevertheless, the transcription factor

most often associated with senescence is NF-κB. It consists of two subunits, p50 and p65 (RelA), and is bound to the inhibitor of NF-κB (IκB) in the inactive state (Figure 1B). Upstream signals from the p38MAPK[63] or the mTOR pathway[56,64] can activate the two associated proteins TAK and TAB.[65] In turn, these activate the IκB kinase (IKK) complex, consisting of the subunits IKKα, IKKβ, and NEMO. After IKK phosphorylates IκB and thereby tags it for degradation, NF-κB is free and can become active. The connection of NF-κB to senescence was clearly shown in a study about genetic regions of SASP genes. Many of the genes contained binding sites for NF-κB and C/EBPß, and were involved in increasing senescence via a positive feedback loop.[55] Despite the importance of the NF-κB pathway for the senescence phenotype, activation of that pathway is not unique to senescent cells. Hence researchers explored a different approach to finding a common signature based on the inflammatory phenotype: the analysis of the SASP composition. Indeed, some inflammatory proteins like IL-6, IL-8, Tnfα and IL-1β[66,67] are often found in the secretome of senescent cells. However, the SASP composition is so unspecific that it cannot be used as a marker[30] - it does not even allow for discrimination between the SASP and any other cell with an NF-κB activated stress response.[25]

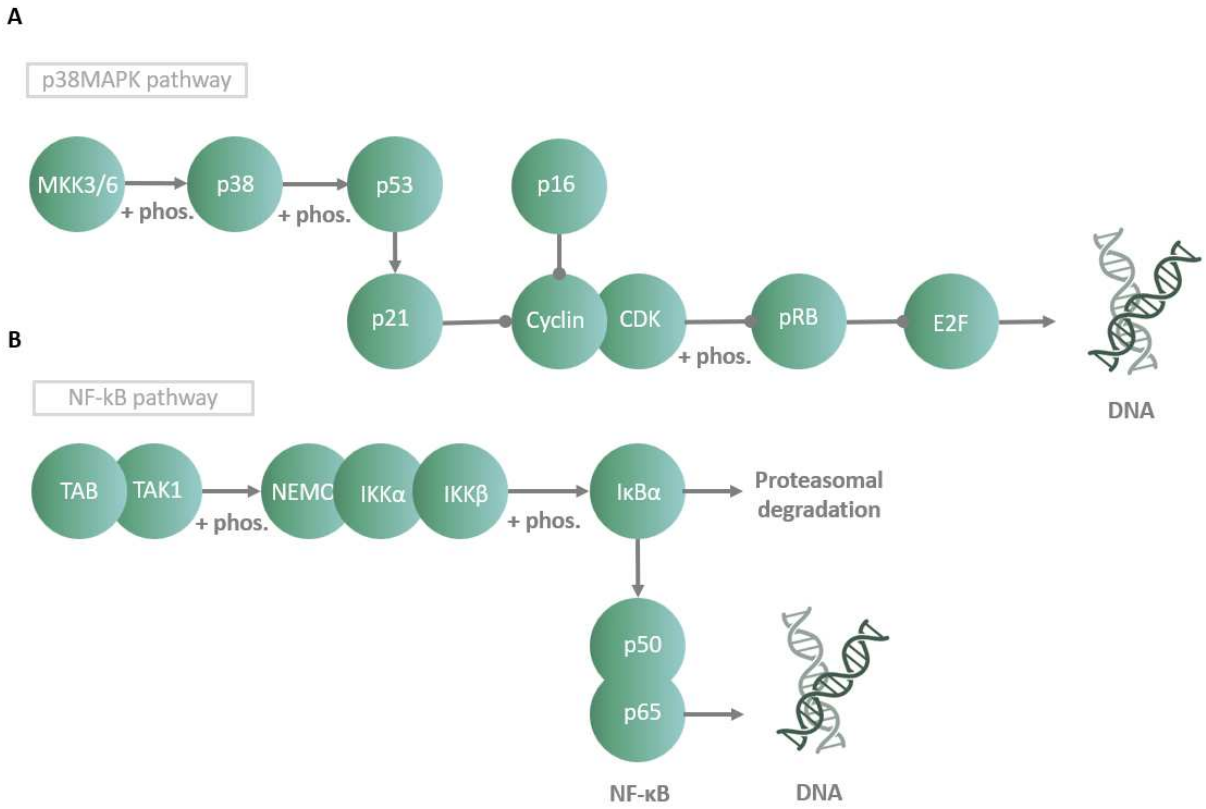

Figure 1. Important pathways in cellular senescence. *(A) p38MAPK pathway (B) Canonical NF-κB pathway. Adapted from KEGG[47] pathway maps.*

ELIMINATION OF SENESCENT CELLS CAN BE AGGRAVATED BY MULTIPLE MECHANISMS

In addition to the pathways involved in senescence, the interaction of the immune system with senescent cells was investigated. Hence, the most prominent interactions described in the literature were summarized. If senescent cells accumulate in a tissue, immune cells are recruited by the SASP, and the damaged cells are cleared by phagocytic cells like macrophages. That way new space for healthy cells is created and the inflammation is resolved. However, in aged tissues or tissues with persistent damage, this process is diminished.[4,68] Even though the exact mechanisms for this are not yet fully understood, three main players will be described. One reason for a rise in senescent cells can simply be a higher rate of accumulation in older age. The other mechanisms are connected to immune surveillance: either the recruiting of immune cells is impaired or the responsible immune cells themselves are less functional at an older age.[4,69] Indeed, it has been known for some time that the function of the immune system decreases with age and it is suspected that these changes result in the accumulation of senescent cells.[70,71] Further, it has been observed that senescent cells can establish an immunosuppressive environment.[72,73] Even if usually the SASP components induce activation of M1-like macrophages that are classically pro-inflammatory[74], they seem to be able to also induce M2-like polarization of macrophages[73]. As M2-like macrophages express tissue repair and anti-inflammatory proteins[75,76] they could even impede the clearance process. That is especially noteworthy as macrophages are currently assumed to be majorly involved in senescence control.[69,74,77] This has also been observed in the liver where monocyte/macrophage-dependent killing of senescent hepatocytes has been demonstrated.[78]

Another way senescent cells can interfere with immune surveillance is through the expression of certain ligands on their cell surface. The main targets of these mechanisms are natural killer (NK) cells and $CD8^+$ T cells, both of which can carry NKG2A receptors.[24] In a study of fibroblasts *in vitro* it was shown that the non-classical MHC class I molecule HLA-E was induced via the p38MAPK pathway after SASP induction. Blocking the interaction of the ligand with the NKG2 receptor on T cells led to enhanced clearance of senescent cells.[24] However, HLA-E is not the only ligand that was found to inhibit $CD8^+$ T cells in clearing the senescent cells. A study using the p16-tdTomato mouse model showed a positive correlation between the SASP and the number of senescent liver cells expressing the ligand PD-L1.[23] Generally, upon interaction with the PD-1 receptor on other cells, PD-L1 is essential for the prevention of immune tolerance and exaggerated immune cell activity.[79] However, in this case, it prevented $CD8^+$ T cells from exerting their cytotoxic action.

THE AGING PROCESS IN THE LIVER WAS CAPTURED IN A SINGLE CELL RESOLUTION

Even though the field of senescence research is accelerating, availability of data for aging related senescence still poses obstacles. For instance, in the plethora of papers, the consensus of using multiple markers for the identification of senescent cells *in vitro* is not always followed. Moreover, investigations are difficult to compare, as different markers are used and hence lead to diverse outcomes. There is also no benchmark data set that is used as a standard for research efforts. Since the immune surveillance is suspected to play an essential role in the accumulation of senescent cells with age, only *in vivo* data can provide adequate information. Even though such studies have been conducted, senescence was induced by irradiation or acute liver damage[39,80] instead of aging. Since *in vitro* studies showed high differences in the outcome depending on the stressor[36,37], it is unlikely that those data sets are representative of an aging phenotype. Additionally, they are limited by the number of time points, due to the more complex experimental setup. Tagging of marker proteins and staining of the tissue is likely to give a good indication of the protein levels but requires many steps that become more elaborate when more markers need to be investigated. These shortcomings can be tackled by using a transcriptomics data set. Even if the transcriptome is not as good of a predictor of what is happening at the protein level, data that has been produced for a different purpose can be easily reused and likely more data points are available. This is shown as the Tabula Muris Senis[46], a single-cell transcriptomic atlas of mouse organs and tissue, encompasses mouse liver cells throughout their lifespan. The time points range from 3 to 30 months, which is equivalent to a range of young adulthood to centenarian age in humans[43] (Figure 2A). In the face of the named limitations, and the good time coverage of this data set, it was deemed the most suitable one to investigate the dynamics of aging-related senescence.

In the data set of the liver are nine different cell types including resident liver cells (hepatocytes, endothelial cells of the hepatic sinusoid, duct epithelial cells, hepatic stellate cells, Kupffer cells) and cells of the immune system (NK cells, plasmacytoid dendritic cells, B cells, myeloid leukocytes) that can migrate to the liver (Figure 2B). Morphologically, the hepatocytes are aligned along sinusoidal capillaries, which contain Kupffer cells. The sinusoids are lined with endothelial cells and are spatially separated from the hepatocytes by the space of Disse, which contains the hepatic stellate cells[67] (Figure 2C). The most strongly represented cell types in the data set are hepatocytes and Kupffer cells with more than 1600 cells each (Figure 2B). With only two duct epithelial cells in the data set, there is a large difference between the number of cells of each cell type. Some additional varieties in the data are the number of cells

per time point and the number of replicates. The time points 3 months and 30 months were strongly represented, but at 24 months only 119 cells were measured (Figure 2D). This variability between the number of cells is even visible within each sample, as the proportions of each cell type show differences (Figure 3). For time points 3 and 30, there were three biological replicates and two for the 24-month time point. However, for the ages of 18 and 21 months, only one mouse was measured. Even though not every time point is represented with the same quality, the single-cell resolution can give valuable insights into marker expression of individual cells throughout the whole life span of a mouse.

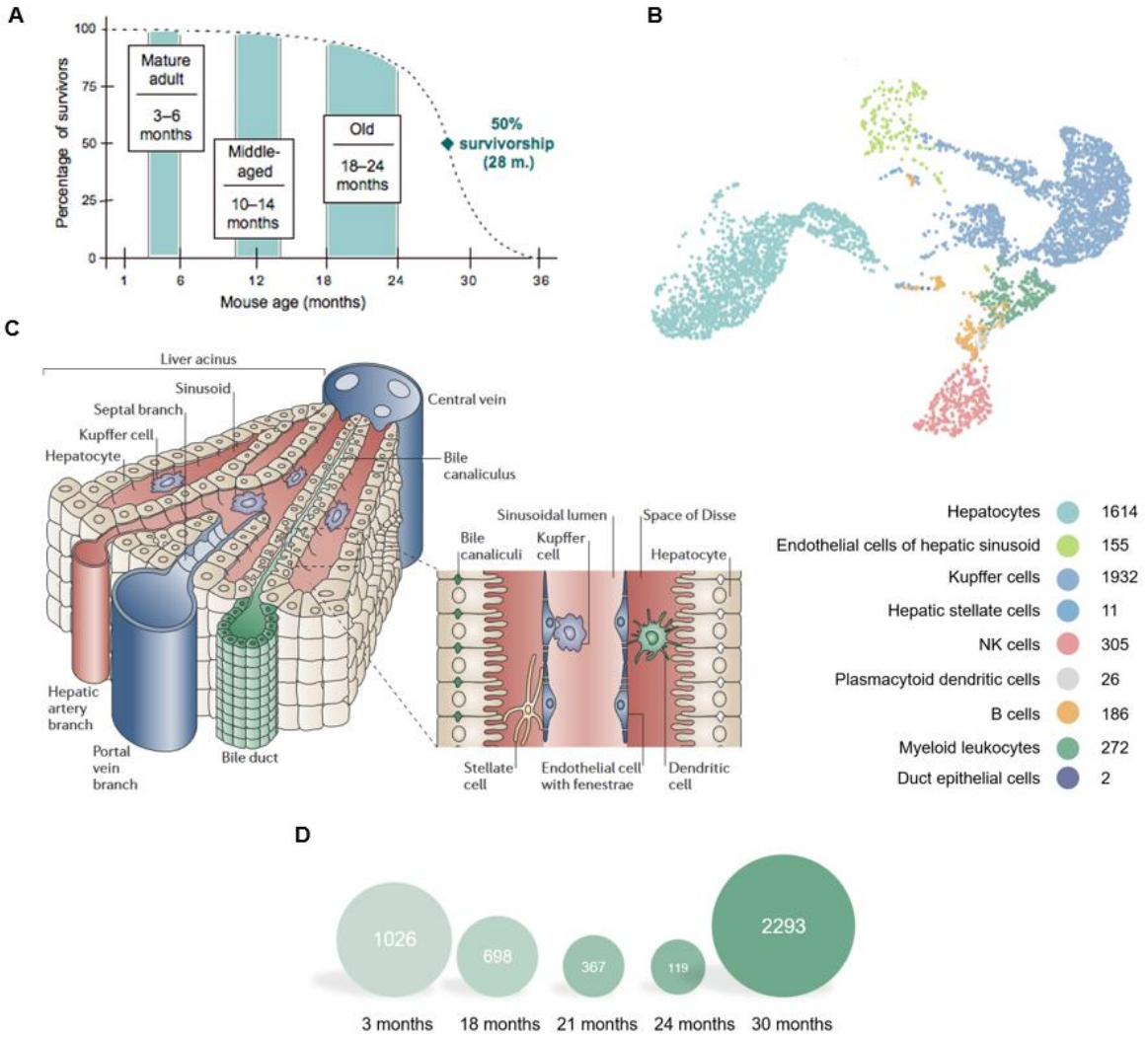

***Figure 2. Characteristics of the single cell transcriptomics data set**. (A) Equivalents of mice to human age, taken from Hagan[43] (B) UMAP of all cells in the data set including number of cells per cell type (C) Liver lobule morphology, taken from Adams et. al[76] (D) Number of cells per age group.*

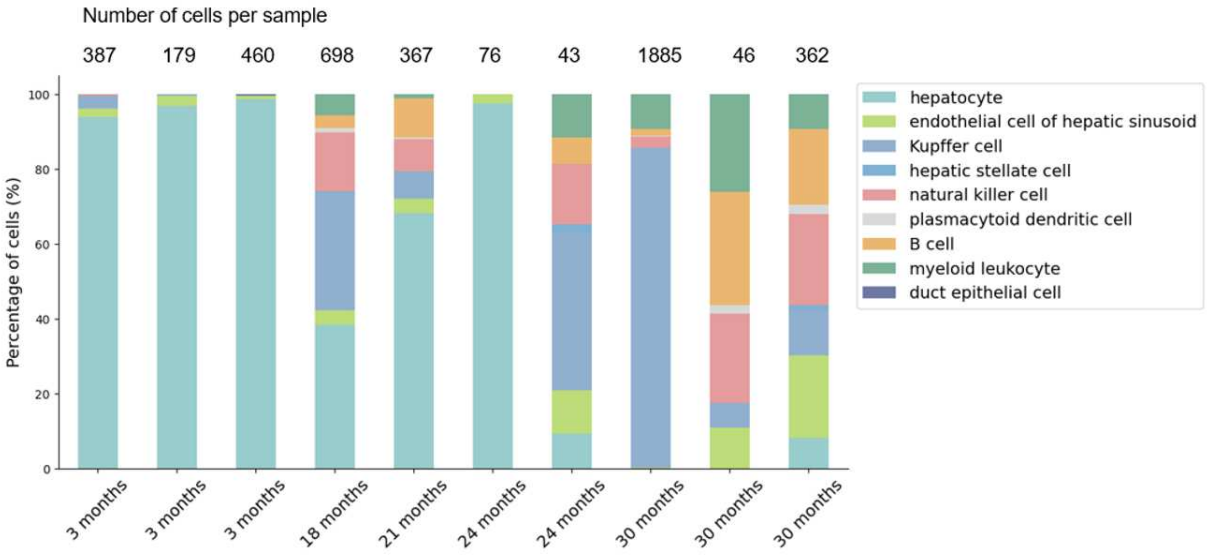

Figure 3. Percentage distribution of cell types in each sample.

THE P38MAPK AND NF-ΚB PATHWAYS ARE INCREASINGLY EXPRESSED OVER TIME

The expression of senescence marker genes is different in every organ[81] and can even vary between livers of different individuals[67]. After a literature search on the most important pathways in senescence, the dynamics of the involved genes were investigated. On that account, the percentage of cells that express the gene was calculated for each time point. As for later analysis only hepatocytes, Kupffer cells and endothelial cells were used, only those were included in this analysis.

Pathways involved in cellular senescence should not be expressed by many cells at the early time points, but show an increase over time, or vice versa. We used the KEGG[47] pathway maps on cellular senescence, NF-κB, PD-L1, Janus kinases - signal transducer and activator of transcription proteins (JAK-STAT), tumor necrosis factor (TNF), and programmed cell death-ligand 1 (PD-L1) as source of information for the pathway structure. An exact overview of the investigated pathways can be found in the appendix (Supplementary figure 1-5). As quality control, we included the housekeeping gene GAPDH[82], which was expressed in over 90 % of the cells at all time points (Supplementary figure 7R, Appendix). From all 18 pathways that were analyzed, there were seven (C, I, J, K, L, M, N) that showed very heterogenous gene

expression dynamics (Figure 4C, Supplementary figure 6, Appendix). Even though in pathway R the genes were similar in their dynamics, the number of cells expressing it, were only minimally increasing (Supplementary figure 7R, Appendix). In contrast, in pathways D and O, the overall trend is increasing (Figure 4D, Supplementary figure 6O, Appendix). However, in both of the pathways, there is at least one gene that, even though essential for the pathway, is only expressed by less than 10 % of the cells at the last time point. Higher expression of a gene is no guarantee for a higher active protein level but presence of RNA is required to increase the protein level. Notably, pathway Q is the only one where a downward trend at the last time point can be observed (Supplementary figure 7Q, Appendix). The pathways E and F exhibit very similar dynamics, because they are both involved in TNF signaling (Figure 4E and Figure 4F). Pathway E describes the activation of NF-κB by TNFα, while F shows the TNFα mediated induction of the p38MAPK pathway. A similar parallel is visible for pathway G and H (Figure 4G and Figure 4H). G portrays the different JAK-STAT genes and H the induction of PD-L1 via interferon gamma (IFNγ) and JAK-STAT. Even though the expression of IFNγ is close to zero, the cytokine could be expressed by the other cells that are not included in this analysis, like immune cells[83].The JAK-STAT pathway (G), includes JAK and STAT isoforms that exhibit distinct functions. According to the pathway map (Supplementary figure 3, Appendix), the rise in JAK1 and STAT3 would allow activation upon binding of inflammatory factors like members of the IL-6 or IL-2 family. The increase of cells expressing the genes of pathway H could indicate the development of a JAK-STAT mediated induction of PD-L1 expression, which can work as a resistance mechanism against immune surveillance[23].

A very homogenous upward trend is visible in pathway A (p38MAPK pathway) (Figure 4A). While in many senescent cells, not only this cell cycle arrest pathway but also the p16 axis is activated, the dynamics of p16 (Cdkn2a) did not mirror that (Figure 4D). An upward trend is also visible for the NF-κB pathway (Figure 4B), which is only disturbed by IKKα (Chuk), which shows a peak at 21 months and decreases thereafter. In contrast, the pathways that the other inflammatory transcription factors c/EBPβ and GATA4 are involved in (Supplementary figure 6N and Supplementary figure 6K), do not show that trend. Altogether, this suggests, that in the hepatocytes, Kupffer cells, and endothelial cells of this data set, cell cycle arrest is exhibited by the p38MAPK/p53 axis, while NF-κB influences the inflammatory phenotype.

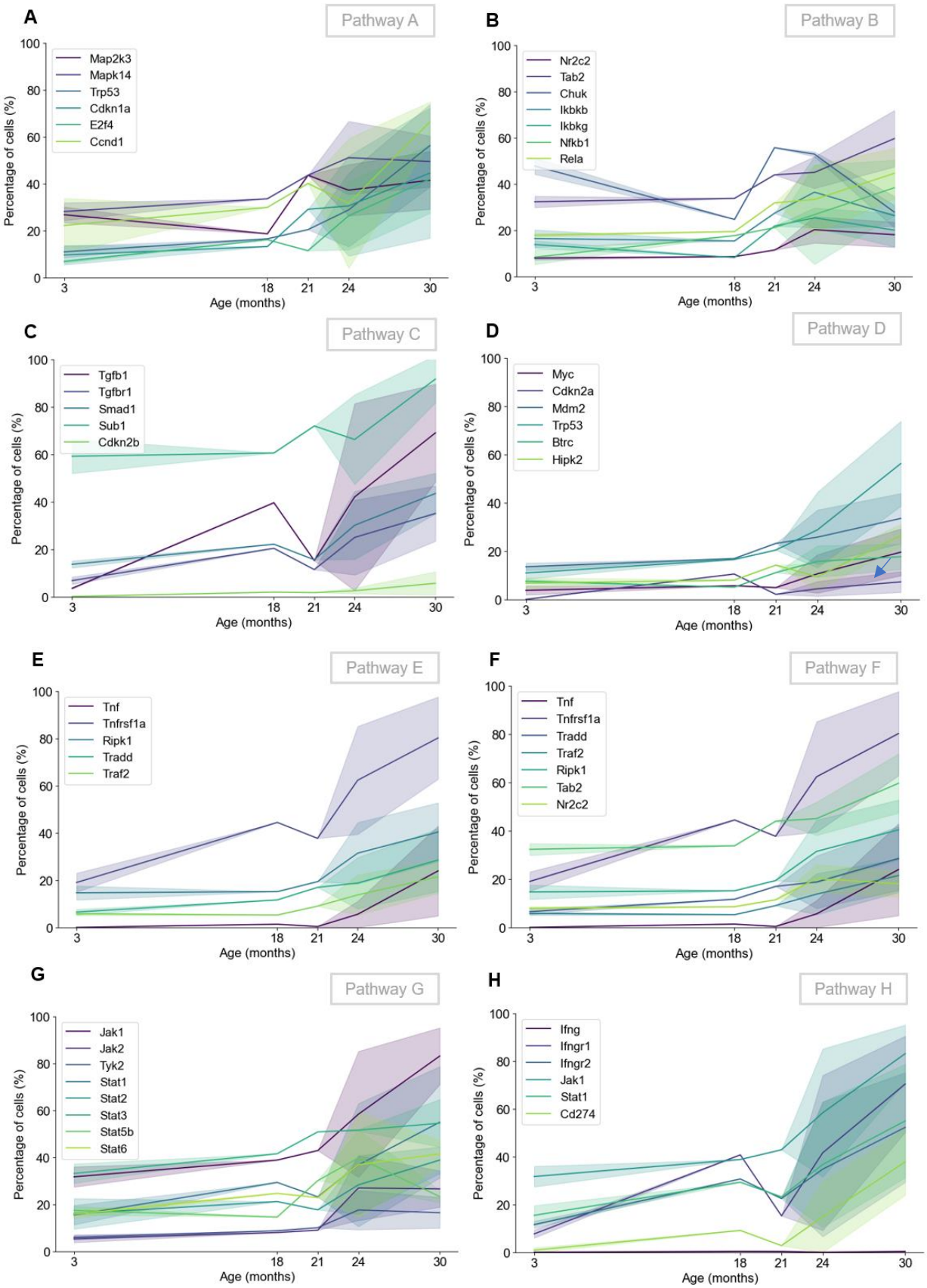

Figure 4. Dynamics of genes in relevant pathways. *Percentage of hepatocytes, Kupffer cells and endothelial cells expressing a gene per timepoint. The corresponding pathway maps are visualized in Supplementary figure 1-5. Conversion of gene names to protein names can be found in Supplementary table 1.*

Dynamic inflammatory proteins are likely regulated by NF-κB

Since the upregulation of the genes can only be shown on a transcriptional level, differential splicing events or post-translational modifications like phosphorylation are not taken into account.[84] As a consequence, there is no control if the pathways are indeed upregulated. To still get an indication, downstream targets of the transcription factors in the pathway were investigated for upregulation. For the p38MAPK pathway, a downstream target is cyclin D (Ccnd1), which is expressed in G1 phase[85]. Indeed, its gene expression showed the same trend as the pathway itself (Figure 4A). The transcription factor NF-κB targets the genes of many SASP components. The KEGG[47] pathway map on cytokines and cytokine receptor interactions offers a broad overview of inflammatory proteins that might be involved, so their dynamics were analyzed. Out of 66, only 15 showed an increase in cells expressing the gene of which 12 were expressed in less than 30 % before 24 months (Supplementary figure 8). However, there might be additional non-cytokines such as adhesion molecules[86] involved. To get an even broader picture, a DGE with all cell types in the dataset was performed. The 30-month-old mice were compared to the 3-month-old ones and the resulting list of the most differentially expressed genes was compared with a list of human inflammatory genes[49]. Out of the 400 most differentially expressed genes, 24 were included in the list of inflammatory genes. As with the cytokines from the pathway map, their dynamics were examined. Since 14 were expressed in more than 40 % of the cells at three months, or reached their highest point at 18 months, they were disregarded (Supplementary figure 8). The other genes were further investigated for the transcription factors targeting them. The most frequent transcription factor was found to be NF-κB, which suggests that indeed NF-κB is increasingly activated and relevant. As a simplification, it was assumed that the influence on inflammation from other pathways outside of p38MAPK and NF-κB is negligible. To stay constant with that assumption, only cytokines from the pathway map and the DGE that are transcriptionally targeted by NF-κB were further used as representatives of SASP (Figure 5). Even though non-cytokine genes were considered in the DGE analysis, none were included in the final SASP compound list. When comparing the dynamics of the NF-kB pathway with the SASP, a different behavior was observed. As the genes were further downstream, the SASP was deemed more representative of inflammation. Therefore, an assembly of the most changed inflammatory proteins to describe inflammation could be established and together with p38MAPK it describes the dynamics of two major hallmarks of senescence.

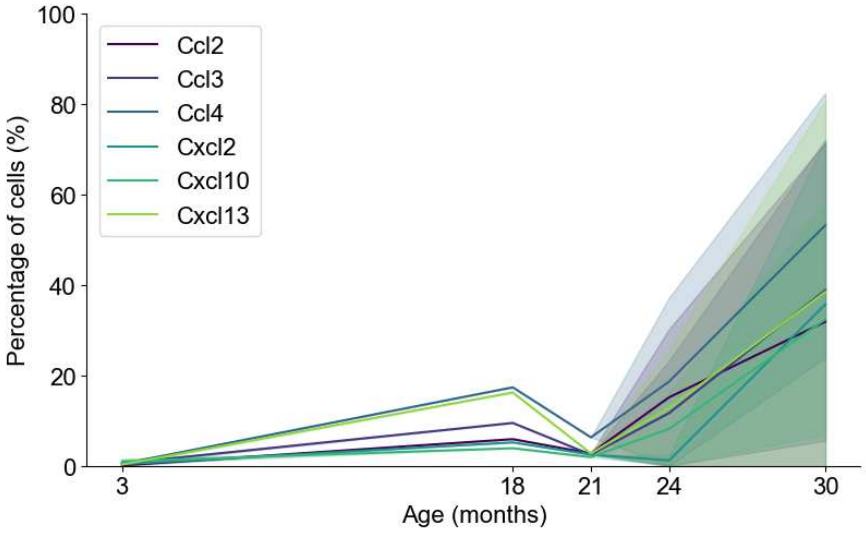

Figure 5. Dynamics of the selected SASP factors. *Cytokines found in the KEGG pathway map and cytokines found in DGE analysis that passed the selection criteria.*

IMMUNE CELL RECRUITMENT COULD NOT BE NOT OBSERVED IN THE DATA

Since the upregulated inflammatory proteins are the mediators that activate the immune system, we hypothesized that a rise in immune cell counts could be visible in the data. Regarding the percentage distribution of all cell types over time (Figure 6), no major change is visible for the non-liver resident immune cells. However, there is an increase of Kupffer cells, which leads to around 70 % of the cells being Kupffer cells at the last time point. Accumulation of macrophages in the liver after injury has previously been observed.[87], as well as macrophages adopting Kupffer cell markers thereafter[88]. Whereas this accumulation could be explained biologically, there is a strong variability between the cell types of samples (Figure 3) that has to be taken into account. Especially since there are only 1 to 3 replicates in this data set, it is difficult to draw conclusions. Therefore, that trend was not regarded as reliable and was not used for further investigations.

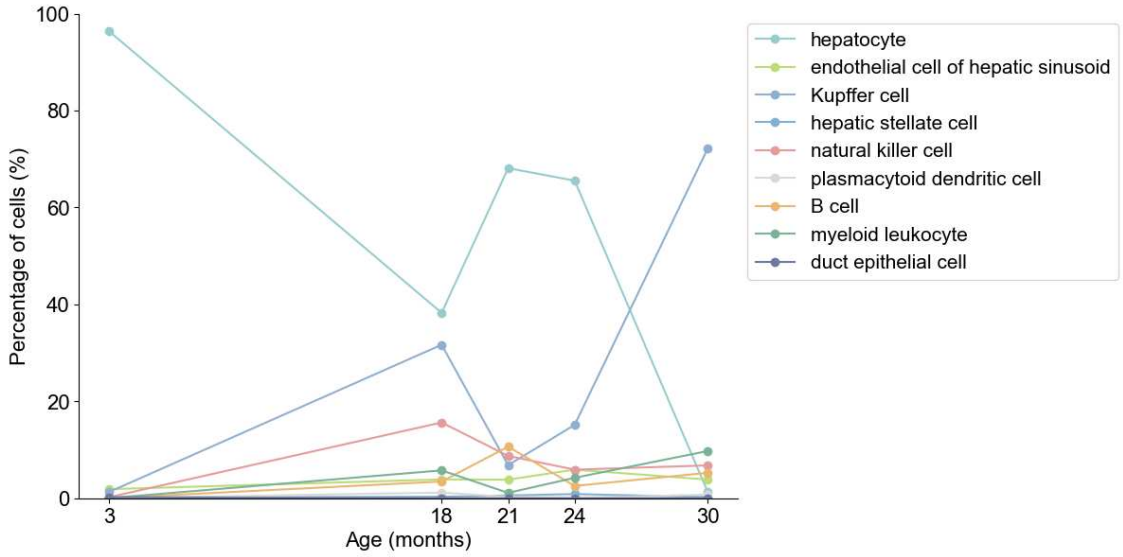

Figure 6. Percentage distribution of all cell types in the data set.

OVERLAP OF KNOWN SENESCENT MARKERS IS RESTRICTED TO ADVANCED AGE

The p38MAPK pathway and the SASP expression are not enough to discriminate senescent cells from non-senescent ones, so quantification methods were investigated. There is a guideline of the International Cell Senescence Association[2] on how to identify senescent cells *in vitro*. Their recommendation is to use a combination of multiple markers, broader ones for screening, followed by verification by co-staining with more specific ones.[89] This strategy can be adapted to the *in silico* setting by selecting cells that express known senescence marker genes. The assumption that among the collected cells in the data are indeed senescent ones, is backed up by the fact senescent cells accumulate with age[90] and less than half of all mice usually survive until the age of 30 months[43]. However, the estimations for the percentage of senescent cells vary substantially depending on the assay that was performed.[91] *In vivo* studies on aged mice, using Senescence-associated beta-galactosidase (SA-β-gal) staining and ImageStreamX for analysis, found a percentage of about 1 to 14 %.[91] These expectations cannot be directly translated to the *in silico* context, as the processing steps can introduce contortions. Nevertheless, it can be assumed that they stay in the minority, and more importantly, that they accumulate with time.

The selected genes for the senescence marker panel included markers for cell cycle arrest, DNA damage, SASP, and others.[92]. There were general markers that were frequently found[66,92]

and more specific SASP combinations from the liver[67] and prostate epithelial cells[18]. The plot (Figure 7A) showed that some markers were expressed by less than 10 % of the cells which is not ideal for finding an overlap. Notably, among them were markers that were classified as general markers. Even if only a small percentage expresses the marker, overlap is possible. However, in this dataset no cells expressing all markers were found. Consequently, the ten markers that were expressed in most cells were tested, which resulted in an overlap of 11 cells. Furthermore, all of those cells were obtained at time point 30, so no information on dynamics could be obtained. Therefore one marker at a time was excluded, to find a set that provides an overlap at most time points. The panel was reduced to TGFβ, IL-18, IL-1β, Cdkn2a, and Gdf15, of which only IL-1β was part of the liver markers. Even after limiting the panel to five markers, there were only four cells at time point 24 and none at 3 months (Figure 7B). The number of positive cells would rise from 4 to 1212 only six months later. This indicates that this approach was not suitable for obtaining senescence dynamics for this data set.

A

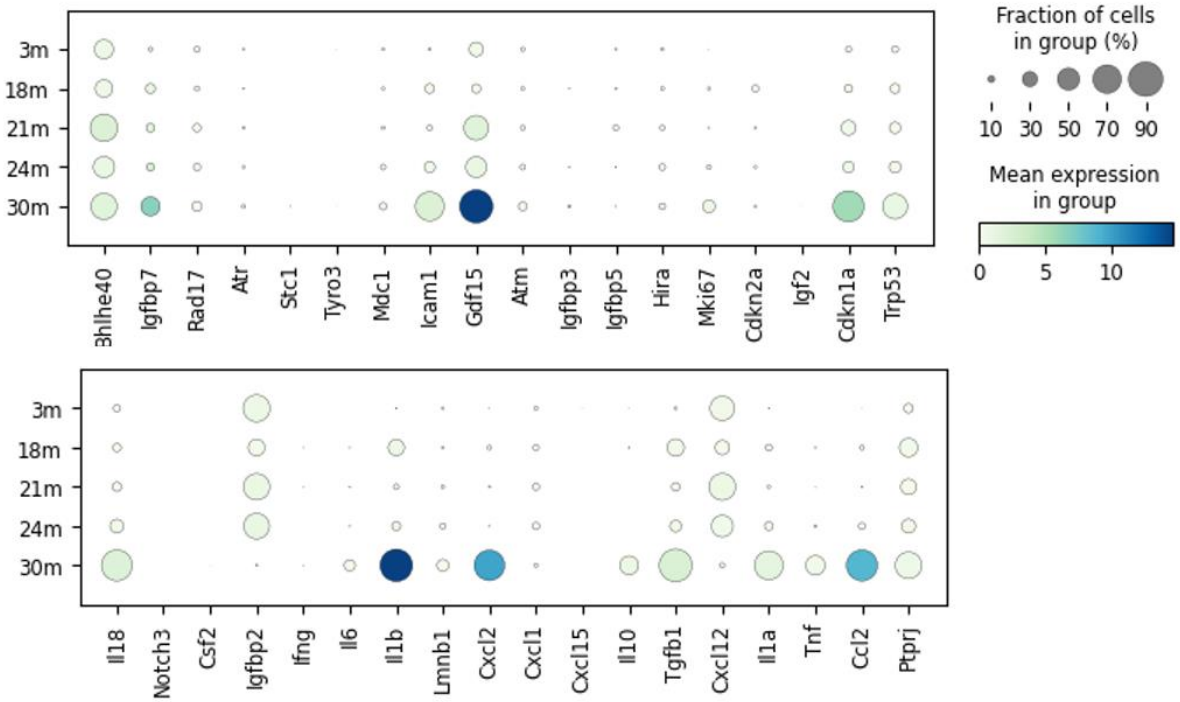

B

Age	3 months	18 months	21 months	24 months	30 months
Number of cells	0	2	1	4	1212

Figure 7. Senescence marker panel. *(A) Marker panel including all investigated markers (B) Number of cells positive for the marker panel including the markers TGFβ, IL-18, IL-1β, Cdkn2a, and Gdf15.*

SENEPY REVEALS DYNAMICS OF SENESCENCE

In addition to the classical marker overlap, *in silico* tools allow for the investigation of more complex relationships in data sets. While DGE is frequently used to find patterns in expression, other methods like dynamic gene correlations can capture the dynamic aspect of senescence. This approach was taken by Sanborn *et al.*[41], who created a tool for quantification of senescence on a single cell level, named Senepy. This package allows the scoring of a data set with pre-generated hubs that indicate the senescence state of the cell. When choosing the data for the hubs, they placed certain requirements on the genes. The expression of the gene had to increase by a certain amount over time and the percentage of cells expressing the gene needed to be less than 1 % in young and between 1 % and 20 % in old cells. These requirements overlap with the strategy that we used in this work for the analysis of the pathways. They further used the selected genes to form networks of correlated genes, called hubs. When we scored the cells with the cell type-specific hubs, the scores obtained were not all in the same range (Figure 8A). The highest scores were obtained from the Kupffer cells, whereas the lowest ones can be observed in the endothelial cells. However, as this score is purely based on the average expression of the genes included in the Senepy hub subtracted by background genes with similar expressions, it does not allow for a meaningful biological interpretation.

To provide a more interpretable measure for the Senepy score, the authors suggested using an individual threshold to classify the cells as either senescent or not. The threshold has to be adjusted to make the number of senescent cells match the expectations. In this work, a cutoff at two standard deviations from the mean Senepy score was used. With this threshold, the percentage of senescent cells stayed between 0 and 20. In contrast to the marker panel, cells were obtained for every time point, but at a low quantity (Figure 8B). The percentage of senescent cells at all time points was calculated to investigate the trend. However, the dynamics of the data did not match the expectations as the percentage of putative senescent cells decreased at the last two time points. When using the average Senepy score instead, an increase over time was obtained (Figure 8C).

A

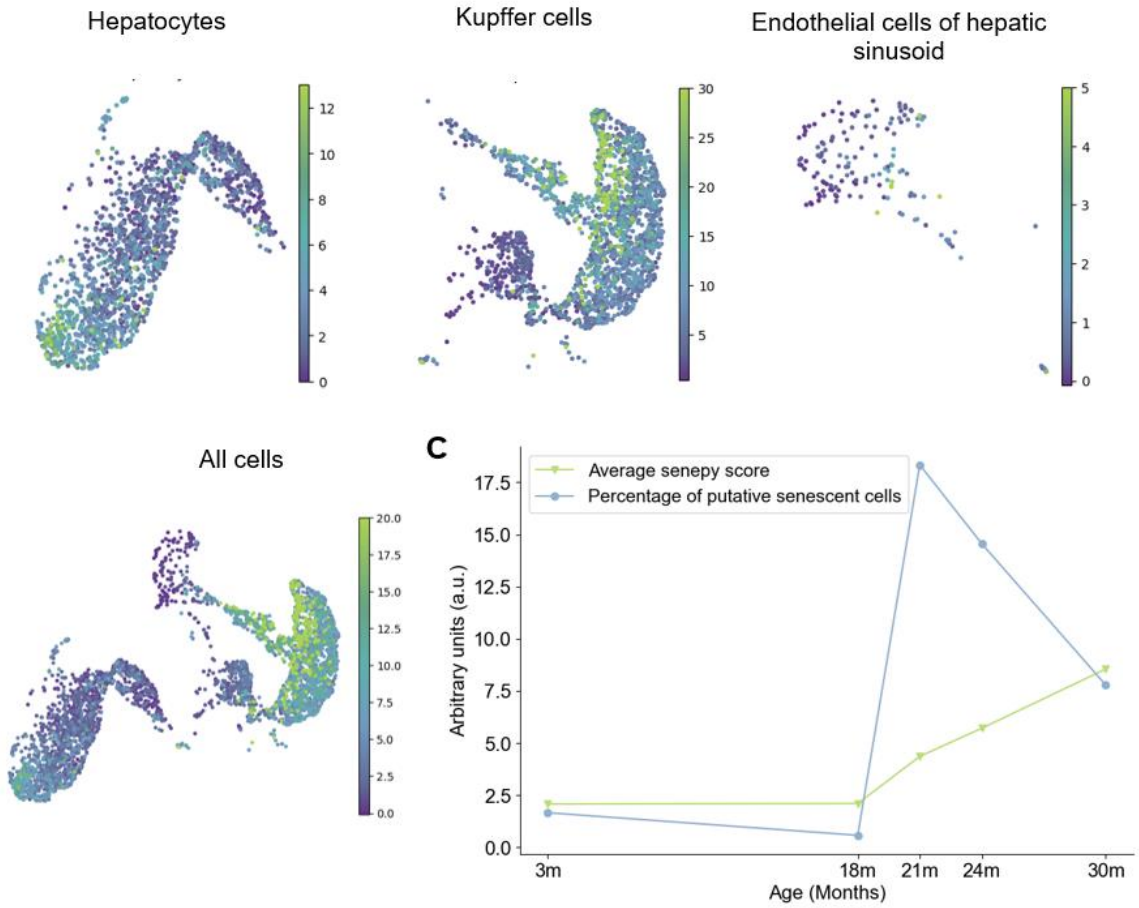

B

Age	3 months	18 months	21 months	24 months	30 months
Number of cells	17	3	53	15	138

Figure 8. Results of scoring the cells with Senepy. *(A) UMAP of cells coloured according to the Senepy score. (B) Number of cells retrieved as putative senescent per time point (C) Dynamics of average Senepy score compared to percentage of putative senescent cells.*

CELL CYCLE ARREST AND INFLAMMATION PATHWAYS SHOW DISTINCT DYNAMICS

Two hallmarks of senescence, the cell cycle arrest and the SASP have shown an increase over time. Additionally, scoring the cells with Senepy has resulted in a measure that relates to senescence at each time point. How those pathways interact and contribute to the rise in senescence can be investigated with an ODE model.

In this model, each of the three variables was described with an ODE. The interactions between the variables were incorporated by adding terms in the equations. The parameters of each equation were fitted to the single-cell data of each pathway. If the equations with the fitted parameters cannot reproduce the dynamics in the data, the anticipated interactions do not sufficiently explain the data and thus the biological interactions. Matching dynamics of the equations and the data indicate that the anticipated interactions are sufficient to describe the data, but are still no guarantee for describing the biological interactions.

To simulate the pathways with ODEs, the single genes in the pathway had to be summarized. The most straightforward way to do so is to calculate the mean of each gene for each time point. However, the sample size of each biological replicate showed big variations. So instead, the weighted average was calculated with the total number of cells per sample as weights. Since the pathway dynamics were based on the percentage of cells and the senescence on the Senepy score, the data had different units and scales. Thus all data points were scaled to a shared highest time point and given an arbitrary unit.

The averaged and scaled pathways and the senescence score are portrayed in Figure 9. All three variables show a moderate increase until time point 18, which is followed by a higher increase thereafter. Notably, a small peak at 21 months in the cell cycle arrest and at 18 months at SASP dynamics, does not follow the overall trend. Since these time points are only represented by one biological replicate, those small variations were regarded as artifacts and therefore not considered essential for the overall dynamics. In the other time points, that had more than one biological replicate, there is a trend in the variability: At three months it is the lowest, and it increases until it is higher at 24 months and biggest at 30 months.

As explained above, it is known that the p38MAPK pathway can regulate the SASP via NF-κB and the outcome of both pathways contributes to the senescence phenotype. When describing this system as dependencies, the connection between the two pathways is straightforward. However, senescence is not a pathway but a phenotype that is connected to the cell cycle arrest and inflammation pathway, which makes it more difficult to anticipate those interactions. In the cell, the effects of the pathways on transcription and the protein levels are visible in the

magnitude of hours.[52] In this data set, however, the time resolution is much lower so it cannot be derived from the data which pathway is activated first and induces the other.

Generally, when looking at the data, all of the variables show a time-dependent increase, but the one in SASP is especially pronounced. This strong rise at the late time points indicates that there is positive feedback involved, either from other variables or SASP itself. Indeed, SASP components like IL-1β lead to positive feedback for the NF-κB pathway.[93] For cell cycle arrest, a feedback loop has been reported as well. ROS lead to p38MAPK induction and if the damage (e.g. caused by telomere attrition) cannot be resolved, ROS are further produced.[94,95] Cells producing ROS or SASP components, can thereby not only reinforce their senescent state but also spread senescence, which is known as paracrine senescence.[96] So the induction of senescence in a cell is dependent on both, its own state, as well as that of its neighboring cells.

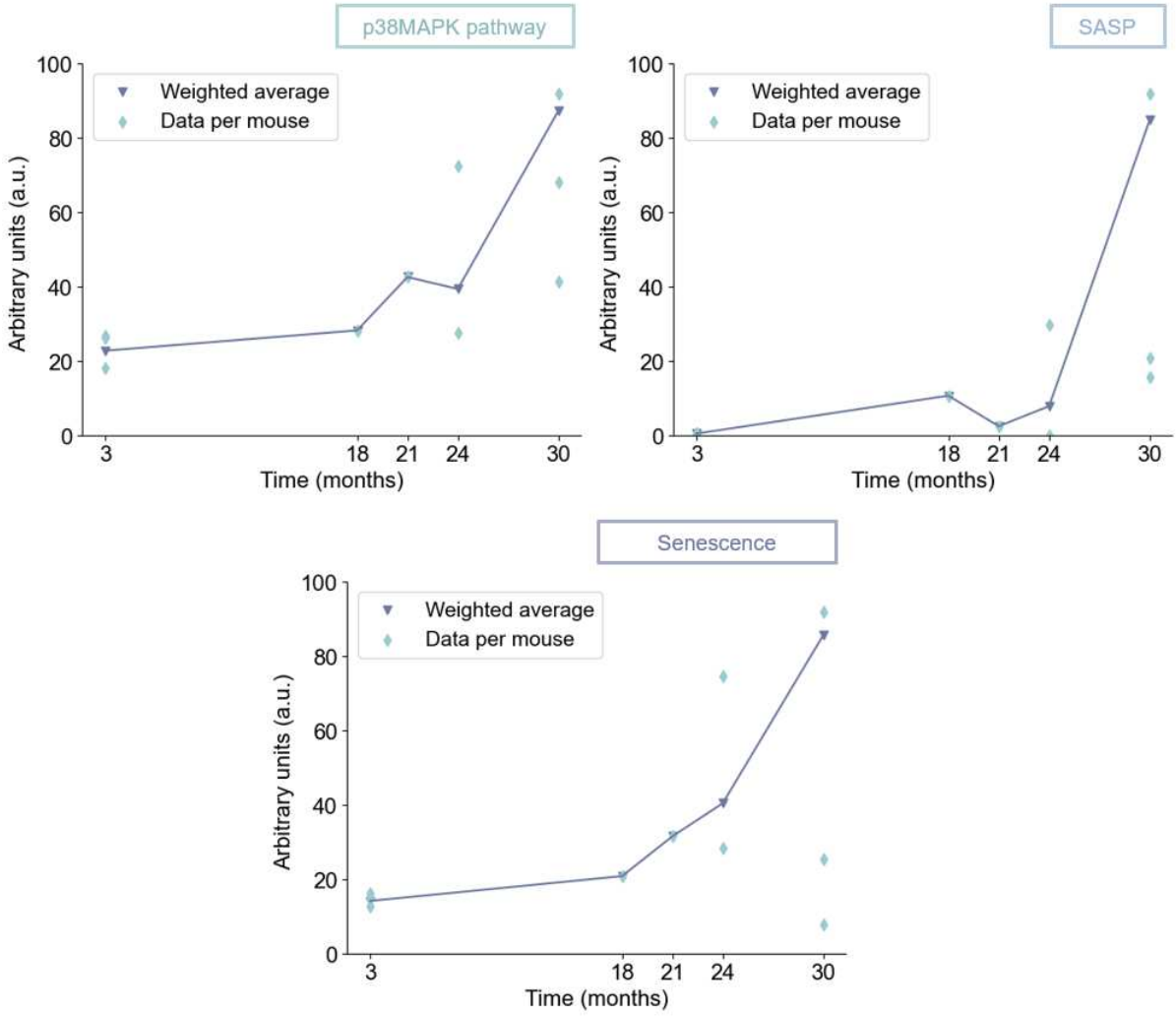

Figure 9. Weighted average of the genes and the Senepy score for each variable in the ODE model.

INCREASING RATE OF P38MAPK INDUCTION IS NECESSARY TO DESCRIBE THE BIOLOGICAL INTERACTIONS

The averaged pathways were used to build models and determine the best qualitative fit. Since the interaction between the p38MAPK pathway and the SASP was already described in literature, in the first step, only the interaction of these two variables was modelled. Each of the equations has a basal induction and a basal degradation rate and both p38MAPK and SASP show positive self-induction. Of course, senescence can also have an impact on the p38MAPK-SASP interaction, but the general dynamic should be describable nonetheless. Indeed, in model A (Figure 10), the trend was decently described, even if the first time point of cell cycle arrest and the last of SASP were not precisely captured.

As a next step, an equation for senescence was added to the model. Initially, it was anticipated that both p38MAPK and SASP have essential positive effects on the rise of senescence. In model B (Figure 10), a good fit was obtained for senescence, but for SASP, the last time point was still not captured. Even if in this model, the first time point of cell cycle arrest could be explained better, that resulted in a flatter dynamic of cell cycle arrest. When analyzing the fitted parameters, an almost equal influence of cell cycle arrest and SASP on senescence was found (Supplementary table 3, Appendix).

Since the steep increase in SASP at the last time point was not explained in model B, it was hypothesized that the rise in senescence could also have an inducing effect on the SASP. Biologically, that assumption is backed up by the principle of paracrine senescence. If there are senescent cells, they can produce SASP themselves and therefore add to the amount of cells expressing SASP. In model C, that hypothesis was tested, but interestingly the simulation of the SASP was even worse (Figure 10).

As alternative hypothesis, it was considered that this paracrine effect of senescence on the SASP is more dominant, so the effect of SASP on senescence becomes negligible. Therefore, in model D (Figure 10), the effect of SASP on senescence was removed. Although decent fits for cell cycle arrest and senescence were achieved, the increase of SASP was not at all captured. This model fit resulted in a negative net induction of SASP (rate of self-induction subtracted by rate of self-inhibition) (Supplementary table 5, Appendix), which shows that the assumptions are not fit to describe the data.

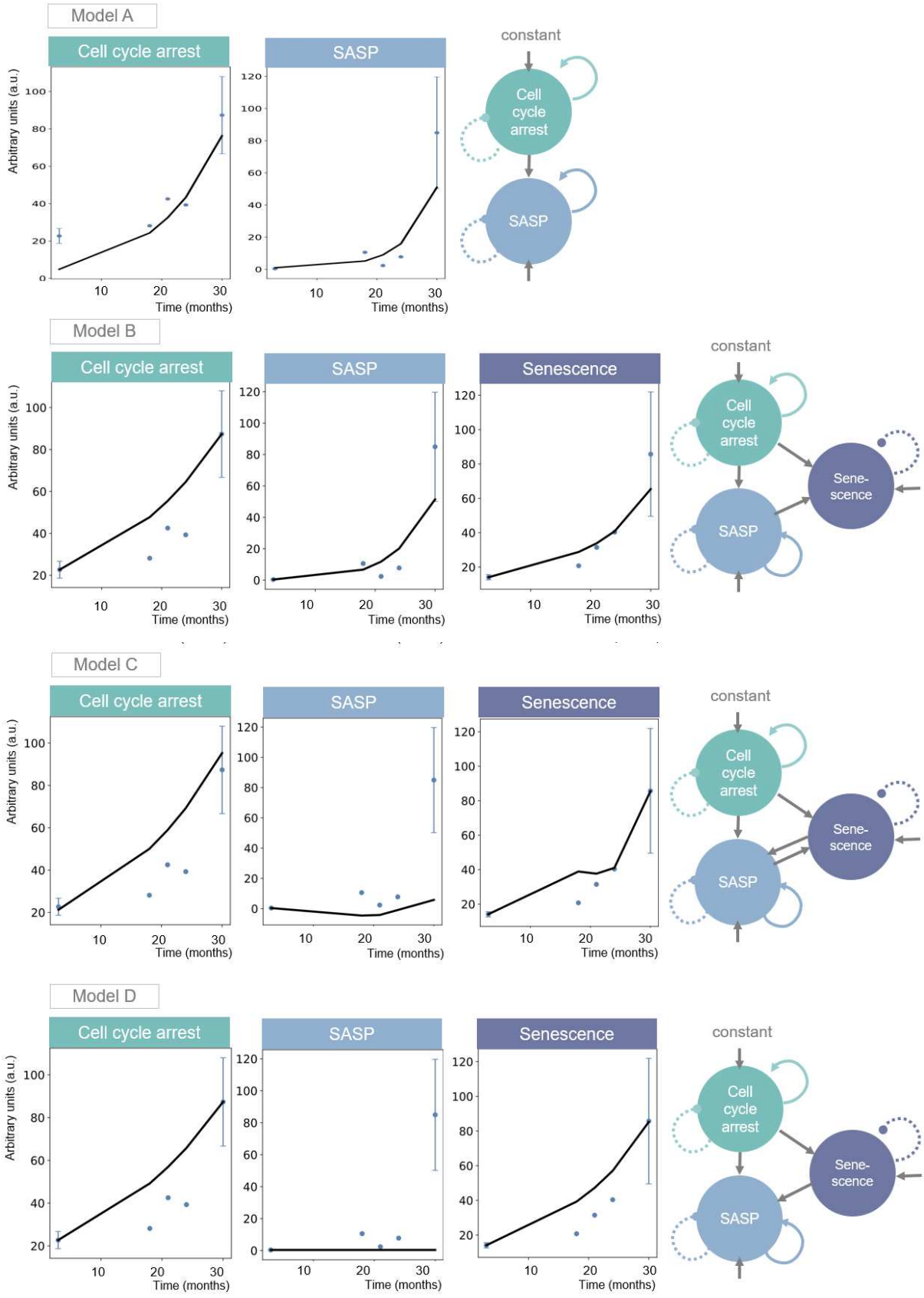

Figure 10. Results of parameter fitting with schematic representations of the models A-D. *Dotted arrows indicate inhibition and full arrows induction.*

For all previous models, it was assumed that the rate of activation of the cell cycle arrest stays constant throughout the lifetime. However, it was hypothesized that stressors like oxidative stress are more prevalent in higher age and therefore induce p38MAPK at a higher rate. This scenario is described in model E (Figure 11). This assumption resulted in a very good fit for senescence and SASP. Cell cycle arrest was well described regarding the first and last time point, but shows a decrease from 3 to 18 months which does not match the dynamics of the original data. In contrast to the previous models, in this one, there was no positive self-induction of SASP included. This could happen in the cell if there are components of the SASP that inhibit the NF-κB pathway as well as stimulating ones. To test whether adding positive induction would improve the fit, model F was created (Figure 11). In this model, a decrease between 3 and 18 months was visible in both cell cycle arrest and SASP. As model E remains the one fitting the data better, that indicates that there are inhibiting factors expressed. These results are also mirrored in the cost, as model E showed the lowest cost in the models with three variables (Table 1). Since none of the scenarios where cell cycle arrest was induced at a constant rate, showed a better fit than model E, that would indicate that a changeable rate of cell cycle arrest induction is important.

To check if even all three variables are needed to describe senescence in the model, the influence of one single variable on senescence was tested. The two models G and H (Figure 11), achieved good fits. Even though this is an oversimplified version of the interactions, with this data it was not possible to prove that the more complex relationships are indeed essential. Therefore, those results highlight that due to the simple dynamics of the data, it might be facilitated to get a good fit and the results have to be interpreted carefully.

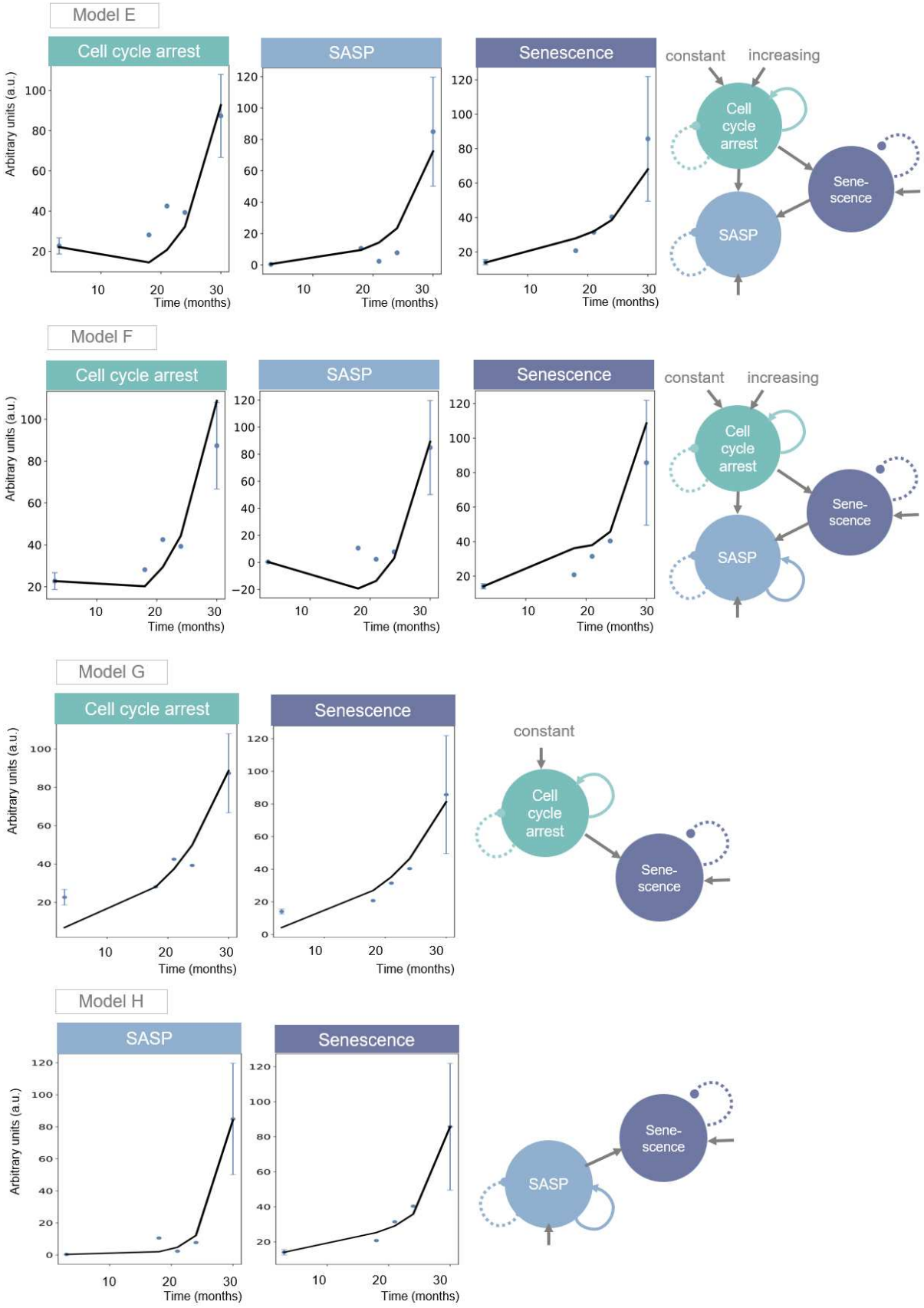

Figure 11. Results of parameter fitting with schematic representations of the models E-H. *Dotted arrows indicate inhibition and full arrows induction.*

Table 1.Overview of all ODE models. *Interactions of cell cycle arrest (CCA), senescence (SEN) and SASP.*

Model	Total cost	Cost per variable	Cycle arrest induction	Description
A	782	391	constant	CCA induces SASP
B	4208	1403	constant	SEN depends of CCA and SASP
C	6570	2190	constant	Positive feedback between SASP and SEN
D	6645	2215	constant	SEN induces SASP
E	3213	1071	increasing	SEN induces SASP
F	4841	1614	increasing	Positive self-induction SASP
G	692	346	constant	SEN depends on CCA
H	404	202	-	SEN depends on SASP

THE BOOLEAN MODEL CAPTURES SIMPLE INTERACTIONS BETWEEN SENESCENT CELLS AND THE IMMUNE SYSTEM

Whereas certain pathways influence senescence on a cellular level, the immune system can interact with senescent cells on a microenvironmental level. In healthy tissue, immune cells are recruited by the SASP and eliminate the damaged cells, to make room for healthy cells. However, in aged tissues, this process is impaired. As laid out above, there are many mechanisms suspected to play a role in the weakened immune surveillance of senescent cells. The scenario where senescent cells develop evasive mechanisms was incorporated into a Boolean model, to portray these interactions in the liver.

A Boolean model consists of a network of nodes that can interact with each other. In this case, most nodes are equivalent to a cell type: senescent cells, senescent cells expressing a resistance marker, and immune cells (T lymphocytes, macrophages). In addition, there is a node that represents an immune suppressive environment. For each node, there are two states: active (1) and inactive/dead (0). In the biological context this model can be interpreted as the perspective of a senescent cell on its microenvironment. Active cells can approach the senescent cell and if they are deactivated, they can be replaced by another one of their type.

In contrast, the senescent cell itself cannot be substituted with another one. A custom function was introduced to ensure that once it has been deactivated/killed, it will remain inactive. The resistant senescent cell in the model caries HLA-E and PD-L1 ligands on its surface that counteract the immune system. The anti-inflammatory macrophage counteracts inflammation, whereas the node pro-inflammatory macrophage stimulates it. The T lymphocyte is representative for $CD8^+$ T cells, carrying NKG2A and PD-1 receptors. Classically, T cells need APCs for antigen presentation and activation, but it was shown that hepatic stellate cells (HSCs), resident liver cells, can take over that task, even if they are less effective.[77] Since the APC function might be substituted by HSCs, APCs were not added as a new cell type. Thus, in the model, the T cells were already activated without having contact with another cell. The connections of all cells and the anti-inflammatory environment was portrayed as a network in Figure 12A. In this representation each cell is a node and every edge is an interaction which can be either stimulating or inhibiting. These interconnections are described with logic rules (Supplementary table 10). In this simplified depiction that each of the nodes is either active or not, their state is dependent on the other nodes that it is connected to. At the beginning of a simulation an initial condition is chosen, and for each following step, the rules are applied to the current states of the nodes. The iteration steps that are taken until the final state is reached are representative of time passing. However, not all biological processes take the same amount of time. There are different ways to introduce time dependence of activation. One is to insert an additional node that separates two nodes. That works for some biological processes such as activation of a T cell by APC.[97] Although, that method is less intuitive for other processes that take longer like activation of the adaptive immune system after a cell becomes senescent. Therefore, in this model a different approach was taken: A function was introduced, that allows to specify the time until a node can be activated. Which of the nodes is updated at each time step is random, but which node it is, influences the dynamics of the simulation afterward, and thus the result of the simulation. That means that the outcome of the simulation varies from simulation to simulation. To show not only one possible scenario (Supplementary figure 9), but a good representation of the most likely outcomes, 200 simulations were run and the outcomes averaged. The final states of the simulation are indicative of the predicted biological circumstances.

The primary goal of building this model of the microenvironment of the senescent cell, was to model scenarios that have been described in literature. If the model describes them well, predictions on new scenarios can be made in further studies. The more known scenarios the rules can be applied to, the stronger is the evidence that the model captures the essential biological interactions. With the final model, it was possible to describe four different scenarios: A) the state of senescence, B) the state of no senescence, C) resistance is formed at the same

time as adaptive immunity becomes active, D) the anti-inflammatory environment is only established at a late time point (Figure 12B).

In scenario A, the state of senescence was simulated. Thus, the senescent cell node was active in the initial state. In the first step the cell activated the macrophages of the innate immune response. After five more timesteps, however, the immune-suppressive environment could switch on which allowes macrophages to polarize into the immune-suppressive type. Then, the adaptive immune response with T lymphocytes was activated. However, during the immune response on the senescent cell, the resistant senescent cell which acts against the macrophages and T lymphocytes could be activated. The resulting state of this scenario showed as expected, a high chance of both senescent cells and resistant ones, immune-suppressive macrophages had formed and the immune suppressive environment was established. In scenario B, the senescent cell was not present in the initial state. Instead, only the immune-suppressive environment was activated, so if the model matched the biology the senescent cell would not be activated. Indeed, there was a strong decrease in the activation of the senescent cell compared to scenario A. In scenarios A and B, it was possible for the immunosuppressive environment to develop after the innate immune response had started but before a robust combination of both innate and adaptive immune responses had been established. In scenario C, the development of resistant senescent cells was now possible as soon as the adaptive immune system could be activated. This resulted in a scenario where most outcomes included a present senescent cell. In scenario D, it was shown that without the occurrence of the anti-inflammatory environment until late in the process, the clearance of senescent cells was successful in most cases.
These scenarios show the dynamics of the interactions between the nodes and it was possible to show a case in which the senescent cell cannot be cleared because it activated the anti-inflammatory environment and the expression of resistance ligands. In the model, activation of the anti-inflammatory environment itself does not lead to the activation of senescent cells. Furthermore, it has been demonstrated that clearance of the senescent cells is more successful without the immune suppressive environment. The contrary has also been shown, if there is not enough time for the immune cells to establish a robust response before the resistant cells occur, the senescent cells will survive.

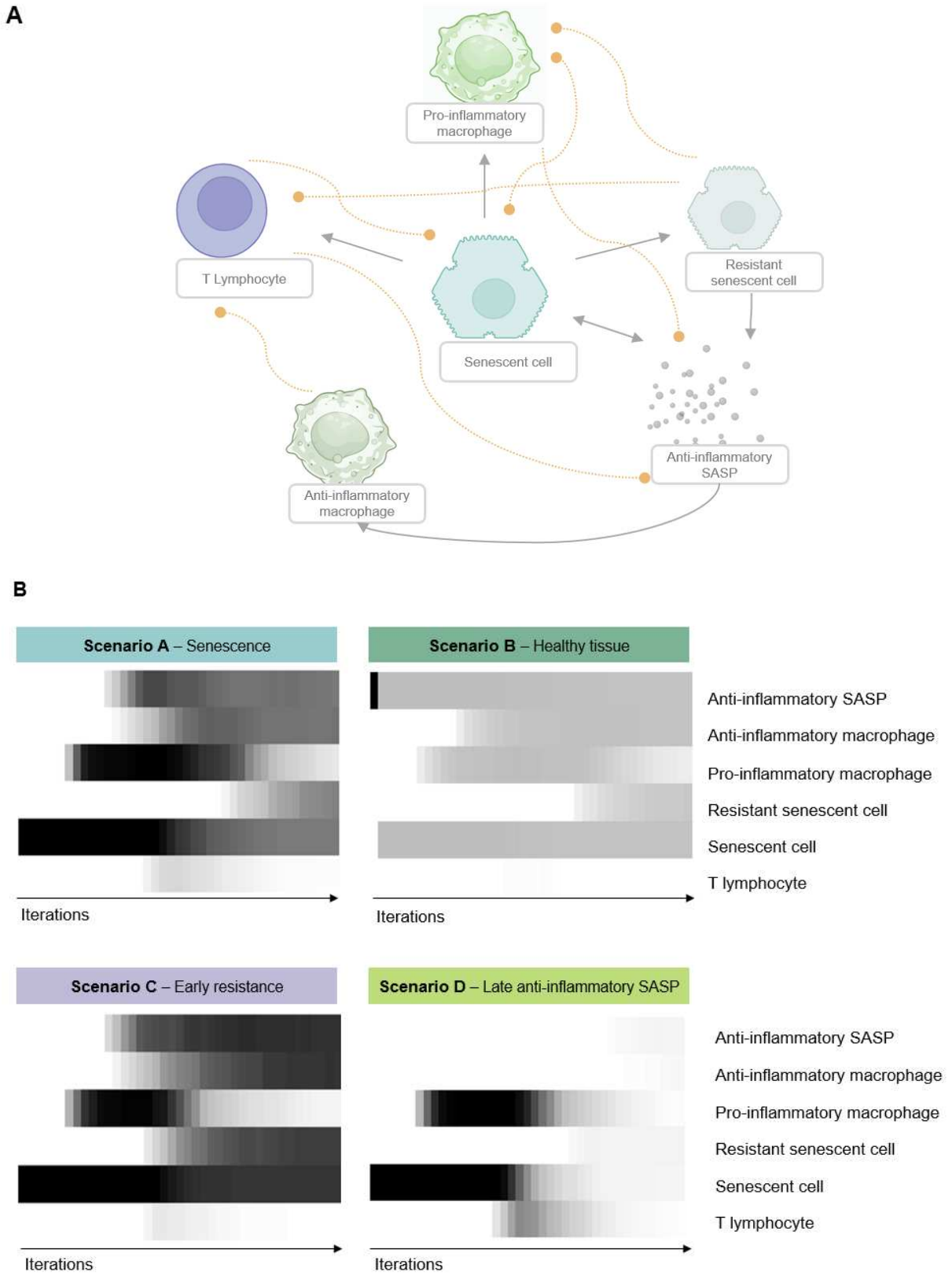

Figure 12. Scheme and simulations of the Boolean model. *(A) Scheme of the Boolean model, orange dotted arrows indicate inhibition, grey full arrows indicate induction. Figure created with BioRender.com (B) Averaged results of 200 simulations over 41 iterations. Black indicates the node is on, white indicates the node is off.*

4

Discussion

Accumulation of senescent cells in the body can contribute to age-related diseases, chronic inflammation, and cancer. Elimination of senescent cells from the body has been proven to increase the healthy life span and ameliorate age-related dysfunctions *in vivo*. To investigate the mechanisms *in vivo*, a single-cell RNA-seq data set was used, containing five time points encompassing the life span of mice.

One of the advantages of the data set was the high resolution of gene expression at single-cell level. Knowing the cell type identities allowed the identification of drifts in expression over time. For example, it became visible that with progressing age, there was a relative increase of Kupffer cells, whereas the fraction of hepatocytes decreased. This drift in the data can have a big impact on the change of gene expression patterns over time. Therefore, the pathway dynamics that were used for the ODE model would include that bias. However, this bias was also introduced by the authors of the data set themselves as they conducted comparisons between marker expressions over time in organs irrespective of the relative cell populations. This heterogeneity between samples could be partially of a biological nature, but since ~70 % of the cells were Kupffer cells at the last time point, a substantial part seems to be introduced by tissue preparation and sequencing. As the cell type percentages do not represent the *in vivo* proportions, it was not possible to incorporate the ratios in the ODE model, for example, to describe the accumulation of immune cells as a result of the SASP. An additional trend in the data was observed: There was an increase of heterogeneity in the expression pattern between individual livers over time. This trend was also witnessed by Nikopoulou *et al*. as they reported a significant increase of heterogeneity with age in single-cell liver transcriptomes.[98] The low number of cells available for time points 18, 21, and 24 was a limiting factor. Therefore, it did not allow for investigation of each cell type separately, to compare transcriptional patterns and infer relationships.

Different pathways can be upregulated in senescence. We were able to identify the p38MAPK pathway and the NF-kB pathway as pathways being expressed in more cells as age progresses. These two pathways are responsible for cell cycle arrest and the secretory

phenotype and therefore essential for cellular senescence. Notably, transcriptomic data is less representative of biological processes than proteomics, which is why we validated the pathways with their downstream target genes. Whereas that was successful for p38MAPK, the NF-kB pathway, showed different dynamics than its downstream targets. Since the pathway is under regulation of post-transcriptional mechanisms like phosphorylation, and proteasomal degradation[99] this can lead to the decoupling of the dynamics. Additional experiments have to be conducted to ensure no bias in expression has been introduced due to the shift in cell types. Even so, the current results suggest that p38MAPK and NF-kB are increasingly activated with age in this liver data set.

Identification and quantification of senescent cells in a transcriptomics data set is challenging. The method used in *in vitro* experiments is selecting cells that are positive for multiple markers. However, in this data set, a panel of known marker genes including ones measured in the liver, was not able to identify any cells that are positive for all markers. The attempts to reduce the panel size down to five resulted in below 10 cells identified at 24 months, which increased to over 1000 cells after 30 months. Senescent cells are expected to accumulate even before 20 months[90] so this identification method did not appear to catch them. This phenomenon of insufficient overlap of markers has also been reported by other researchers[41] and highlights the heterogeneity of senescent cells. Another challenge with the marker panel was that it includes markers that are part of the pathways, like p21. Especially if the panel is limited to a small number of markers, the measures for the pathway and senescence would not be independent when used in a model. Therefore, this approach for quantifying senescent cells remained unsuccessful.

Some markers frequently associated with senescent liver were not increasingly expressed in the data. Among them are the SASP components IL-6 and IL-8[96] but also one of the most widely used markers for senescence, p16 (Cdkn2a). P16 was expressed by the highest percentage of cells at 18 months and less afterward, which does not follow the expected increase. There are several reasons why this might be the case. Firstly, as mentioned above, even in the same organ or cell type, different marker expressions are possible. Secondly, the levels of p16 protein and transcriptomics have not always correlated in the past[35,100], due to technical constraints like gene dropout during the sequencing process. Therefore, missing p16 was not considered a strong contradiction.

As characterizing senescent cells is a common issue in the scientific community, Sanborn *et al.*[41] have developed a data-driven technique to identify senescent cells in single-cell transcriptomic data. Scoring the data with this Senepy method resulted in the anticipated rise of the score with time. Since they also used the Tabula Muris Senis to assemble those hubs,

one could assume that this result can be solely traced back to data-specific genes. However, they validated their hubs on other data sets where they performed better than single markers at identifying senescent cells. As it outperformed the marker panel, this method was chosen, even though further validation of the Senepy method, especially regarding the liver hubs, is essential for providing better reliability.

Although the average senescence score at each time point increased over time, the percentage of senescent cells went down at the last time point. This could be traced back to the way the hubs were calculated. For cell types that had less than 200 cells at the last time point, expressions of the 24-month timepoint were used instead, which was the case for hepatocytes. It might also be a result of the difference between the sample sizes at the different time points. We could still obtain the anticipated upward trend by using the average Senepy score per time point. However, this suitable dynamic came with a tradeoff: The Senepy score is a statistical measure without a unit and could therefore not be interpreted in a meaningful biological way. This abstractness was also reflected in the observation that the score had a different scale for each cell type. As a result, high scores had a bigger relative influence on the mean score. In this case, the highest scores were obtained from Kupffer cells. The more pronounced change reflected in the score might be an indication that Kupffer cells become less efficient at eliminating senescent cells in their surroundings. Although, how far this is translatable to a biological context, still needs to be investigated.

Notably, Sanborn *et al.* just selected genes for their hubs that were upregulated over time. This preference for upregulated genes is reflected in literature, as out of the markers used in the marker panel, only Lamin B1 was expected to decrease in senescence. It might be important to fill that gap about downregulated markers, as clues about crucial interactions could be lost.

To broaden the mechanistic understanding of the accumulation of senescent cells in the liver, we used the information we gained on the data set to build an ODE model. The model is based on three variables: p38MAPK pathway, SASP, and senescence. Interestingly, the model that was able to fit the data best, required an increasing rate of stimulation of the p38MAPK pathway. This does not match our expectations, as telomere attrition, one of the main drivers of aging-related senescence increases in a rather linear manner.[101] Of course, other stressors involved in the process like oxidative stress or DNA damage[102] could accumulate increasingly at high age and therefore contribute to the acceleration. For accumulation of senescence, there is a rate of cells becoming senescent and a lower rate of senescent cells being eliminated. Cell cycle arrest is involved in cells becoming senescent but not in the elimination, whereas SASP is involved in both. The model suggested that cell cycle arrest, but not SASP

is involved in the accumulation of senescence. This would mean that cells become senescent as a result of damage that is independent of paracrine SASP signaling. The rise in SASP expression was induced by the rise in senescence. The accumulation of senescent cells with a secretory phenotype is likely to lead to an overall increase in SASP production. Overall, it became clear that the data dynamics are too simple to provide a sufficient basis for distinct ODE models, as cell cycle arrest and SASP could explain the senescence accumulation independently of each other. The fitting process was also hindered because the ODEs were not identifiable. Since the terms inducing the variable as well as inhibiting it were separately defined in the equations, there are multiple sets of parameters that could fit the optimum.

The immune system also plays an important role in the accumulation of senescent cells with age. We were able to build a literature-based small-scale Boolean model of the microenvironment of a senescent cell. With this model, we were able to portray four distinct scenarios, that matched our expectations. However, the complexity of the model is very low and therefore not close enough to reality to allow meaningful predictions. For example, in this model, the T lymphocyte node represents both NK cells and $CD8^+$ T cells that are positive for NKG2A and PD-1. Furthermore, it has been shown that the macrophages clearing senescent cells in the liver are dependent on $CD4^+$ T cells[78], which is not the case in this model. Here, the anti-inflammatory SASP was summarized into one node, but a separate node for each component could be introduced. The addition of pro-inflammatory components counteracting the anti-inflammatory ones and inducing certain immune cell types would also be valuable for future additions to the model. SASP compound additions could for example be the cytokines identified in the single-cell transcriptomics data. In this model, the goal was only to capture a simple level of known interactions of the immune surveillance of senescent cells, but the end goal would be to visualize the population dynamics of senescent cells. To achieve that, nodes that lead to the growth of the senescent population via paracrine signaling or independent stress events could be added, as previously shown in a model of immunogenic cell death[97]. With this addition, it could deliver estimates for population sizes and could work as a valuable addition to the ODE model.

In brief, two mathematical models describing senescence in liver tissue were successfully built. The Boolean model can be regarded as a solid base for further refinement, which can provide valuable predictive insights into immune interactions and resistance mechanisms. The results of the ODE model indicated that even though the period and amount of time points covered in the data set exceeded the one in previous studies, the resolution was not high enough to describe the data with a distinct model. As the increasing expression of two main

senescence pathways was visible in the transcriptomic data, the transcriptomics seemed to be a sufficient estimation to describe the changes. With always-improving technology, sequencing at a single-cell resolution will become more affordable. Perhaps soon an extension to the Tabula Muris Senis will include more time points for a higher resolution, especially at the earlier stages. More cells at the existing time points would also make it possible to correct for variability and exclude certain cells to get a more balanced ratio of cell types at each age. To sum up, the models and the obstacles that were discovered in the process provide valuable insights into the current state of cellular senescence research and can be used as the foundation for further modeling approaches.

REFERENCES

1. Li, C., Liu, Z. & Shi, R. A comprehensive overview of cellular senescence from 1990 to 2021: A machine learning-based bibliometric analysis. *Front. Med.* **10**, 1072359 (2023).
2. Gorgoulis, V. *et al.* Cellular Senescence: Defining a Path Forward. *Cell* **179**, 813–827 (2019).
3. Kim, S. & Kim, C. Transcriptomic Analysis of Cellular Senescence: One Step Closer to Senescence Atlas. *Mol. Cells* **44**, 136–145 (2021).
4. Muñoz-Espín, D. & Serrano, M. Cellular senescence: from physiology to pathology. *Nat. Rev. Mol. Cell Biol.* **15**, 482–496 (2014).
5. Storer, M. *et al.* Senescence Is a Developmental Mechanism that Contributes to Embryonic Growth and Patterning. *Cell* **155**, 1119–1130 (2013).
6. Muñoz-Espín, D. *et al.* Programmed Cell Senescence during Mammalian Embryonic Development. *Cell* **155**, 1104–1118 (2013).
7. Rajagopalan, S. & Long, E. O. Cellular senescence induced by CD158d reprograms natural killer cells to promote vascular remodeling. *Proc. Natl. Acad. Sci.* **109**, 20596–20601 (2012).
8. Hayflick, L. The limited in vitro lifetime of human diploid cell strains. *Exp. Cell Res.* **37**, 614–636 (1965).
9. Ben-Porath, I. & Weinberg, R. A. The signals and pathways activating cellular senescence. *Int. J. Biochem. Cell Biol.* **37**, 961–976 (2005).
10. Aravinthan, A. D. & Alexander, G. J. M. Senescence in chronic liver disease: Is the future in aging? *J. Hepatol.* **65**, 825–834 (2016).
11. Serrano, M. & Blasco, M. A. Putting the stress on senescence. *Curr. Opin. Cell Biol.* **13**, 748–753 (2001).
12. Lanna, A., Henson, S. M., Escors, D. & Akbar, A. N. The kinase p38 activated by the metabolic regulator AMPK and scaffold TAB1 drives the senescence of human T cells. *Nat. Immunol.* **15**, 965–972 (2014).

13. Campisi, J. Aging, Cellular Senescence, and Cancer. *Annu. Rev. Physiol.* **75**, 685–705 (2013).
14. Fagagna, F. d'Adda D. *et al.* A DNA damage checkpoint response in telomere-initiated senescence. *Nature* **426**, 194–198 (2003).
15. Hara, E. Finding the point of no return for cellular senescence. *Nat. Cell Biol.* **26**, 176–176 (2024).
16. Demaria, M. *et al.* An Essential Role for Senescent Cells in Optimal Wound Healing through Secretion of PDGF-AA. *Dev. Cell* **31**, 722–733 (2014).
17. Chen, X. *et al.* Epithelial cell senescence induces pulmonary fibrosis through Nanog-mediated fibroblast activation. *Aging* **12**, 242–259 (2019).
18. Coppé, J.-P. *et al.* Senescence-Associated Secretory Phenotypes Reveal Cell-Nonautonomous Functions of Oncogenic RAS and the p53 Tumor Suppressor. *PLoS Biol.* **6**, e301 (2008).
19. Krizhanovsky, V. *et al.* Senescence of Activated Stellate Cells Limits Liver Fibrosis. *Cell* **134**, 657–667 (2008).
20. Nathan, C. & Ding, A. Nonresolving Inflammation. *Cell* **140**, 871–882 (2010).
21. Ray, D. & Yung, R. Immune senescence, epigenetics and autoimmunity. *Clin. Immunol.* **196**, 59–63 (2018).
22. Yousefzadeh, M. J. *et al.* An aged immune system drives senescence and ageing of solid organs. *Nature* **594**, 100–105 (2021).
23. Wang, T.-W. *et al.* Blocking PD-L1–PD-1 improves senescence surveillance and ageing phenotypes. *Nature* **611**, 358–364 (2022).
24. Pereira, B. Senescence surveillance: the interplay between the immune system and senescent cells. (UCL (University College London), 2019).
25. Sharpless, N. E. & Sherr, C. J. Forging a signature of in vivo senescence. *Nat. Rev. Cancer* **15**, 397–408 (2015).
26. Sharpless, N. E. & DePinho, R. A. How stem cells age and why this makes us grow old. *Nat. Rev. Mol. Cell Biol.* **8**, 703–713 (2007).

27. Martin, N., Beach, D. & Gil, J. Ageing as developmental decay: insights from p16INK4a. *Trends Mol. Med.* **20**, 667–674 (2014).
28. Signer, R. A. J. & Morrison, S. J. Mechanisms that Regulate Stem Cell Aging and Life Span. *Cell Stem Cell* **12**, 152–165 (2013).
29. Pajvani, U. B. *et al.* Fat apoptosis through targeted activation of caspase 8: a new mouse model of inducible and reversible lipoatrophy. *Nat. Med.* **11**, 797–803 (2005).
30. Hernandez-Segura, A., Nehme, J. & Demaria, M. Hallmarks of Cellular Senescence. *Trends Cell Biol.* **28**, 436–453 (2018).
31. Soto-Gamez, A. & Demaria, M. Therapeutic interventions for aging: the case of cellular senescence. *Drug Discov. Today* **22**, 786–795 (2017).
32. Nacarelli, T. & Sell, C. Targeting metabolism in cellular senescence, a role for intervention. *Mol. Cell. Endocrinol.* **455**, 83–92 (2017).
33. Xie, J., Wang, X. & Proud, C. G. mTOR inhibitors in cancer therapy. *F1000Research* **5**, 2078 (2016).
34. Amor, C. *et al.* Senolytic CAR T cells reverse senescence-associated pathologies. *Nature* **583**, 127–132 (2020).
35. Hernandez-Segura, A. *et al.* Unmasking Transcriptional Heterogeneity in Senescent Cells. *Curr. Biol.* **27**, 2652-2660.e4 (2017).
36. Gasek, N. S., Kuchel, G. A., Kirkland, J. L. & Xu, M. Strategies for targeting senescent cells in human disease. *Nat. Aging* **1**, 870–879 (2021).
37. Casella, G. *et al.* Transcriptome signature of cellular senescence. *Nucleic Acids Res.* **47**, 7294–7305 (2019).
38. MacParland, S. A. *et al.* Single cell RNA sequencing of human liver reveals distinct intrahepatic macrophage populations. *Nat. Commun.* **9**, 4383 (2018).
39. Ashmore-Harris, C. *et al.* Utilising an in silico model to predict outcomes in senescence-driven acute liver injury. *bioRxiv* 2023–10 (2023).
40. Thorgersen, E. B. *et al.* The Role of Complement in Liver Injury, Regeneration, and Transplantation. *Hepatology* **70**, 725–736 (2019).

41. Sanborn, M. A., Wang, X., Gao, S., Dai, Y. & Rehman, J. SenePy: Unveiling the Cell-Type Specific Landscape of Cellular Senescence through Single-Cell Analysis in Living Organisms. *bioRxiv* 2023–08 (2023).
42. Hemedan, A. A., Niarakis, A., Schneider, R. & Ostaszewski, M. Boolean modelling as a logic-based dynamic approach in systems medicine. *Comput. Struct. Biotechnol. J.* **20**, 3161–3172 (2022).
43. Hagan, C. When are mice considered old? *JAX Blog* https://www.jax.org/news-and-insights/jax-blog/2017/november/when-are-mice-considered-old (2017).
44. Rhinn, M., Ritschka, B. & Keyes, W. M. Cellular senescence in development, regeneration and disease. *Development* **146**, dev151837 (2019).
45. CZ Biohub. Tabula Muris Senis data set. https://cellxgene.cziscience.com/collections/0b9d8a04-bb9d-44da-aa27-705bb65b54eb.
46. The Tabula Muris Consortium *et al.* A single-cell transcriptomic atlas characterizes ageing tissues in the mouse. *Nature* **583**, 590–595 (2020).
47. Ogata, H. *et al.* KEGG: Kyoto encyclopedia of genes and genomes. *Nucleic Acids Res.* **27**, 29–34 (1999).
48. National Library of Medicine. National Center for Biotechnology Information Gene data base. https://www.ncbi.nlm.nih.gov/gene/.
49. CD Genomics, D. P. Custom Human Inflammation Panel Gene List. https://ngspanel.cd-genomics.com/wp-content/themes/diseasepanel/pdf/main/custom-human-inflammation-panel-gene-list.pdf.
50. Badia-i-Mompel, P., Dimitrov, D., Holland, C. & Garcia-Alonso, L. DoRothEA.
51. Plaisier, C. L. *et al.* Causal Mechanistic Regulatory Network for Glioblastoma Deciphered Using Systems Genetics Network Analysis. *Cell Syst.* **3**, 172–186 (2016).
52. Heldring, M. M. *et al.* Model-based translation of DNA damage signaling dynamics across cell types. *PLOS Comput. Biol.* **18**, e1010264 (2022).
53. Virtanen, P. *et al.* SciPy 1.0: fundamental algorithms for scientific computing in Python. *Nat. Methods* **17**, 261–272 (2020).

54. Müssel, C., Hopfensitz, M. & Kestler, H. A. BoolNet—an R package for generation, reconstruction and analysis of Boolean networks. *Bioinformatics* **26**, 1378–1380 (2010).
55. Martínez-Zamudio, R. I., Robinson, L., Roux, P.-F. & Bischof, O. SnapShot: Cellular Senescence Pathways. *Cell* **170**, 816-816.e1 (2017).
56. Sikora, E., Bielak-Zmijewska, A. & Mosieniak, G. A common signature of cellular senescence; does it exist? *Ageing Res. Rev.* **71**, 101458 (2021).
57. Romanov, S. R. *et al.* Normal human mammary epithelial cells spontaneously escape senescence and acquire genomic changes. *Nature* **409**, 633–637 (2001).
58. Pajalunga, D. *et al.* Critical requirement for cell cycle inhibitors in sustaining nonproliferative states. *J. Cell Biol.* **176**, 807–818 (2007).
59. Herbig, U., Jobling, W. A., Chen, B. P. C., Chen, D. J. & Sedivy, J. M. Telomere Shortening Triggers Senescence of Human Cells through a Pathway Involving ATM, p53, and p21CIP1, but Not p16INK4a. *Mol. Cell* **14**, 501–513 (2004).
60. Ohanna, M. *et al.* Senescent cells develop a PARP-1 and nuclear factor-κB-associated secretome (PNAS). *Genes Dev.* **25**, 1245–1261 (2011).
61. Kang, C. *et al.* The DNA damage response induces inflammation and senescence by inhibiting autophagy of GATA4. *Science* **349**, aaa5612 (2015).
62. Kuilman, T. *et al.* Oncogene-Induced Senescence Relayed by an Interleukin-Dependent Inflammatory Network. *Cell* **133**, 1019–1031 (2008).
63. Sun, Y., Wang, X., Liu, T., Zhu, X. & Pan, X. The multifaceted role of the SASP in atherosclerosis: from mechanisms to therapeutic opportunities. *Cell Biosci.* **12**, 74 (2022).
64. Wang, D. *et al.* The interactions between mTOR and NF-κB: A novel mechanism mediating mechanical stretch-stimulated osteoblast differentiation. *J. Cell. Physiol.* **236**, 4592–4603 (2021).
65. Takaesu, G. *et al.* TAB2, a Novel Adaptor Protein, Mediates Activation of TAK1 MAPKKK by Linking TAK1 to TRAF6 in the IL-1 Signal Transduction Pathway. *Mol. Cell* **5**, 649–658 (2000).

66. Li, X. *et al.* Inflammation and aging: signaling pathways and intervention therapies. *Signal Transduct. Target. Ther.* **8**, 239 (2023).
67. Yousefzadeh, M. J. *et al.* Tissue specificity of senescent cell accumulation during physiologic and accelerated aging of mice. *Aging Cell* **19**, e13094 (2020).
68. Serrano, M. Senescence Helps Regeneration. *Dev. Cell* **31**, 671–672 (2014).
69. Elder, S. S. & Emmerson, E. Senescent cells and macrophages: key players for regeneration? *Open Biol.* **10**, 200309 (2020).
70. Liu, Z. *et al.* Immunosenescence: molecular mechanisms and diseases. *Signal Transduct. Target. Ther.* **8**, 200 (2023).
71. Lanna, A. *et al.* A sestrin-dependent Erk–Jnk–p38 MAPK activation complex inhibits immunity during aging. *Nat. Immunol.* **18**, 354–363 (2017).
72. Ruhland, M. K. *et al.* Stromal senescence establishes an immunosuppressive microenvironment that drives tumorigenesis. *Nat. Commun.* **7**, 11762 (2016).
73. Mazzoni, M. *et al.* Senescent thyrocytes and thyroid tumor cells induce M2-like macrophage polarization of human monocytes via a PGE2-dependent mechanism. *J. Exp. Clin. Cancer Res.* **38**, 208 (2019).
74. Lujambio, A. *et al.* Non-Cell-Autonomous Tumor Suppression by p53. *Cell* **153**, 449–460 (2013).
75. Gordon, S. & Martinez, F. O. Alternative Activation of Macrophages: Mechanism and Functions. *Immunity* **32**, 593–604 (2010).
76. Adams, D. H. & Eksteen, B. Aberrant homing of mucosal T cells and extra-intestinal manifestations of inflammatory bowel disease. *Nat. Rev. Immunol.* **6**, 244–251 (2006).
77. Prata, L. G. P. L., Ovsyannikova, I. G., Tchkonia, T. & Kirkland, J. L. Senescent cell clearance by the immune system: Emerging therapeutic opportunities. *Semin. Immunol.* **40**, 101275 (2018).
78. Kang, T.-W. *et al.* Senescence surveillance of pre-malignant hepatocytes limits liver cancer development. *Nature* **479**, 547–551 (2011).

79. Kythreotou, A., Siddique, A., Mauri, F. A., Bower, M. & Pinato, D. J. PD-L1. *J. Clin. Pathol.* **71**, 189–194 (2018).
80. Fielder, E. *et al.* Short senolytic or senostatic interventions rescue progression of radiation-induced frailty and premature ageing in mice. *eLife* **11**, e75492 (2022).
81. Idda, M. L. *et al.* Survey of senescent cell markers with age in human tissues. *Aging* **12**, 4052–4066 (2020).
82. Barber, R. D., Harmer, D. W., Coleman, R. A. & Clark, B. J. GAPDH as a housekeeping gene: analysis of GAPDH mRNA expression in a panel of 72 human tissues. *Physiol. Genomics* **21**, 389–395 (2005).
83. Ni, L. & Lu, J. Interferon gamma in cancer immunotherapy. *Cancer Med.* **7**, 4509–4516 (2018).
84. Hegde, P. S., White, I. R. & Debouck, C. Interplay of transcriptomics and proteomics. *Curr. Opin. Biotechnol.* **14**, 647–651 (2003).
85. Yuan, X. *et al.* SARS coronavirus 7a protein blocks cell cycle progression at G0/G1 phase via the cyclin D3/pRb pathway. *Virology* **346**, 74–85 (2006).
86. Albelda, S. M., Smith, C. W. & Ward, P. A. Adhesion molecules and inflammatory injury. *FASEB J.* **8**, 504–512 (1994).
87. Karlmark, K. R. *et al.* Hepatic recruitment of the inflammatory Gr1 $^{+}$ monocyte subset upon liver injury promotes hepatic fibrosis. *Hepatology* **50**, 261–274 (2009).
88. Bonnardel, J. *et al.* Stellate Cells, Hepatocytes, and Endothelial Cells Imprint the Kupffer Cell Identity on Monocytes Colonizing the Liver Macrophage Niche. *Immunity* **51**, 638-654.e9 (2019).
89. Gil, J. The challenge of identifying senescent cells. *Nat. Cell Biol.* **25**, 1554–1556 (2023).
90. Burd, C. E. *et al.* Monitoring Tumorigenesis and Senescence In Vivo with a p16INK4a-Luciferase Model. *Cell* **152**, 340–351 (2013).
91. Biran, A. *et al.* Quantitative identification of senescent cells in aging and disease. *Aging Cell* **16**, 661–671 (2017).

92. González-Gualda, E., Baker, A. G., Fruk, L. & Muñoz-Espín, D. A guide to assessing cellular senescence *in vitro* and *in vivo*. *FEBS J.* **288**, 56–80 (2021).
93. Serasanambati, M. & Chilakapati, S. R. Function of Nuclear Factor Kappa B (NF-kB) in Human Diseases-A Review. *South Indian J. Biol. Sci.* **2**, 368 (2016).
94. Zhang, X. *et al.* Isoliensinine induces apoptosis in triple-negative human breast cancer cells through ROS generation and p38 MAPK/JNK activation. *Sci. Rep.* **5**, 12579 (2015).
95. Passos, J. F. *et al.* Feedback between p21 and reactive oxygen production is necessary for cell senescence. *Mol. Syst. Biol.* **6**, 347 (2010).
96. Acosta, J. C. *et al.* A complex secretory program orchestrated by the inflammasome controls paracrine senescence. *Nat. Cell Biol.* **15**, 978–990 (2013).
97. Checcoli, A. *et al.* Dynamical Boolean Modeling of Immunogenic Cell Death. *Front. Physiol.* **11**, 590479 (2020).
98. Nikopoulou, C. *et al.* Spatial and single-cell profiling of the metabolome, transcriptome and epigenome of the aging mouse liver. *Nat. Aging* **3**, 1430–1445 (2023).
99. Magnani, M., Crinelli, R., Bianchi, M. & Antonelli, A. The Ubiquitin-Dependent Proteolytic System and other Potential Targets for the Modulation of Nuclear Factor-kB (NF-kB). *Curr. Drug Targets* **1**, 387–399 (2000).
100. Marthandan, S. *et al.* Conserved Senescence Associated Genes and Pathways in Primary Human Fibroblasts Detected by RNA-Seq. *PLOS ONE* **11**, e0154531 (2016).
101. Tamura, Y. *et al.* Telomere attrition in beta and alpha cells with age. *AGE* **38**, 61 (2016).
102. Childs, B. G., Durik, M., Baker, D. J. & Van Deursen, J. M. Cellular senescence in aging and age-related disease: from mechanisms to therapy. *Nat. Med.* **21**, 1424–1435 (2015).

APPENDIX

PATHWAY MAPS

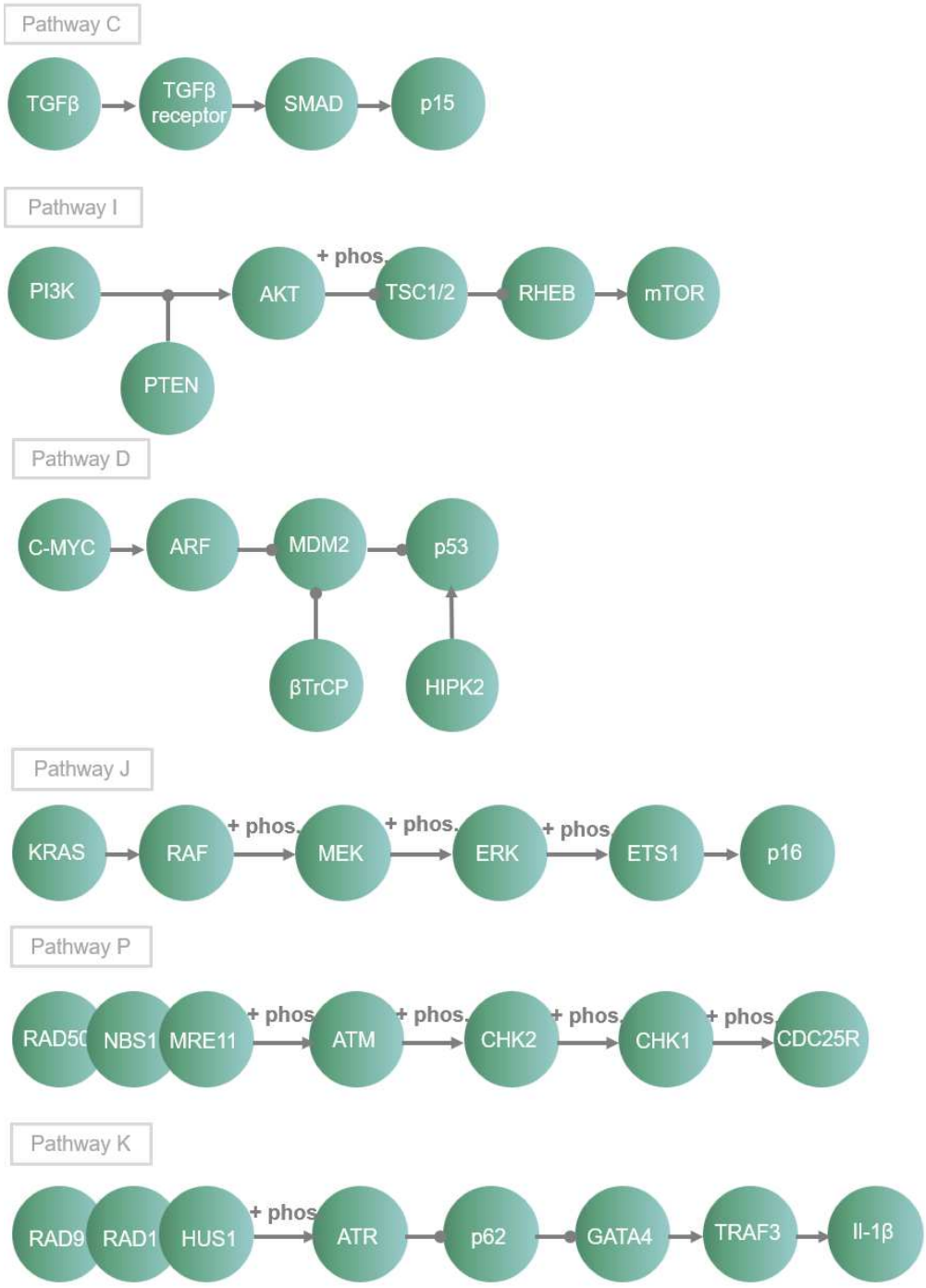

Supplementary figure 1. Pathways from cellular senescence map.

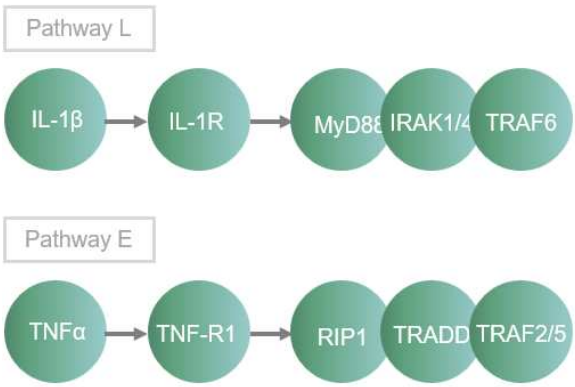

Supplementary figure 2. Pathways from the NF-kB map.

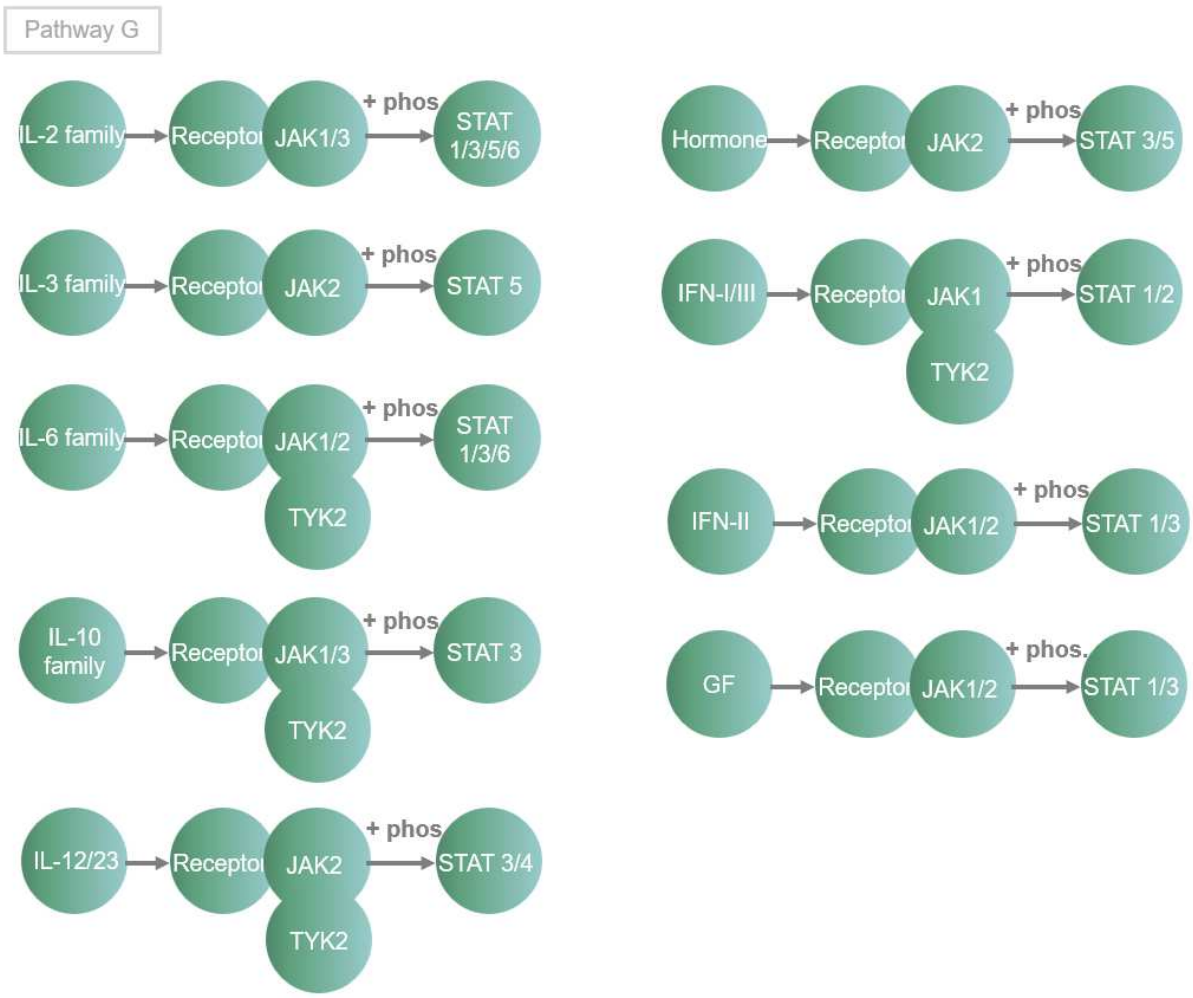

Supplementary figure 3. Pathways from the JAK-STAT map.

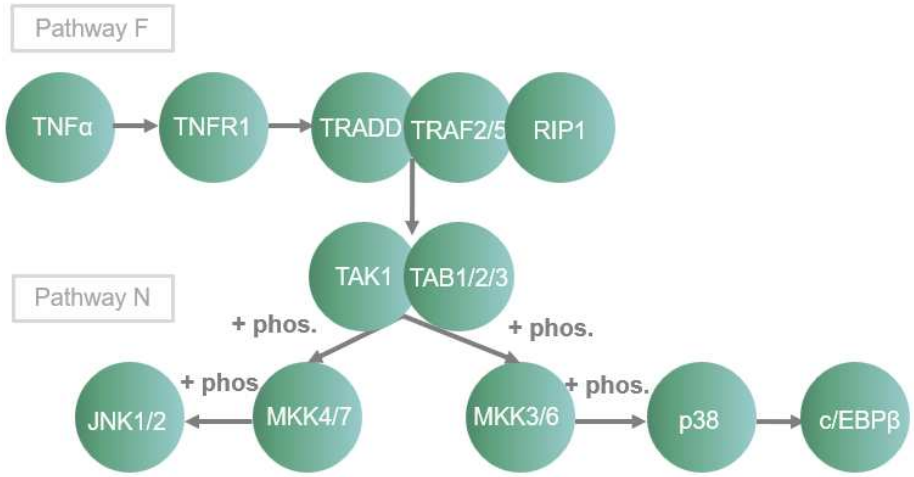

Supplementary figure 4. Pathways from the TNF map.

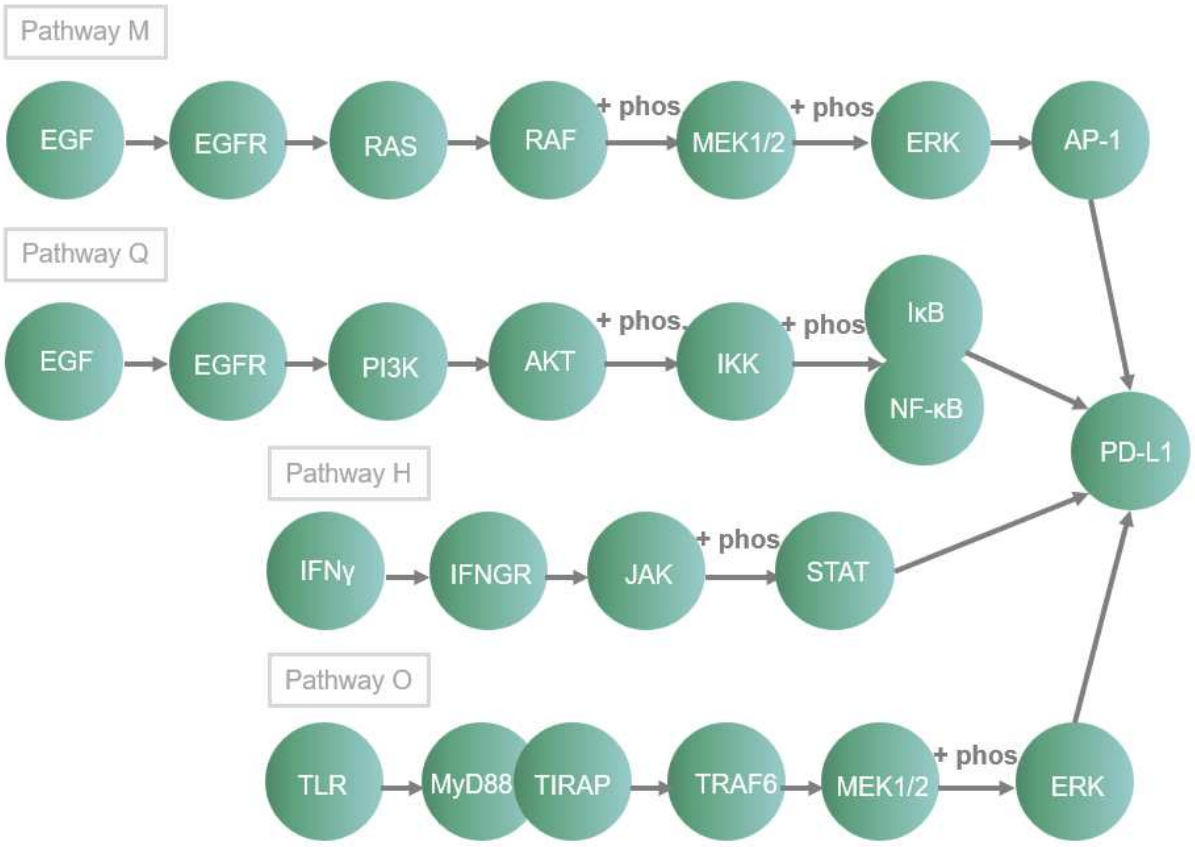

Supplementary figure 5. Pathways from the PD-L1 map.

Supplementary table 1. *Conversion of human protein names to mouse gene names.*

KEGG pathway proteins	NCBI gene name	KEGG pathway proteins	NCBI gene name	KEGG pathway proteins	NCBI gene name
AKT	Akt1	JAK1	Jak1	RAF	Raf1
AP-1	Cd274	JAK2	Jak2	RAS	Kras
ARF	Cdkn2a	JAK3	Jak3	RHEB	Rheb
ATM	Atm	KRAS	Kras	RIP1	Rik1
ATR	Atr	MDM2	Mdm2	SMAD	Smad1
βTrCP	Btrc	MEK	Mdk	STAT1	Stat1
CDC25R	Cdc25a	MEK1	Map2k1	STAT2	Stat2
CHK1	Chek1	MRE11	Mre11a	STAT3	Stat3
CHK2	Chek2	mTOR	Mtor	STAT5	Stat5b
C-Myc	Myc	NBS1	Nbn	STAT6	Stat6
Cyclin D	Ccnd1	p15	Cdkn2b	TGFβ	Tgfb1
E2F	E2F4	p16	Cdkn2a	TGFβ receptor	Tgfbr1
EGF	Egf	p21	Cdkn1a	TIRAP	Tnfrsf1a
EGFR	Egfr	p53	Trp53	TLR	Tlr
ERK	Mapk1	p62	Sqstm1	TRADD	Tradd
ETS1	Ets1	PD-L1	Cd274	TRAF3	Traf3
GATA4	Gata4	PI3K	Pik3cb	TRAF6	Traf6
HIPK2	Kipk2	PTEN	Pten	TSC2	Tsc2
IFNGR	Ifngr1, Ifngr2	RAD1	Hus1	TYK2	Tyk2
IFNγ	Ifng	RAD50	Rad50	RAF	Raf1
IL-1β	Il1b	RAD9	Rad9b, Rad9a		

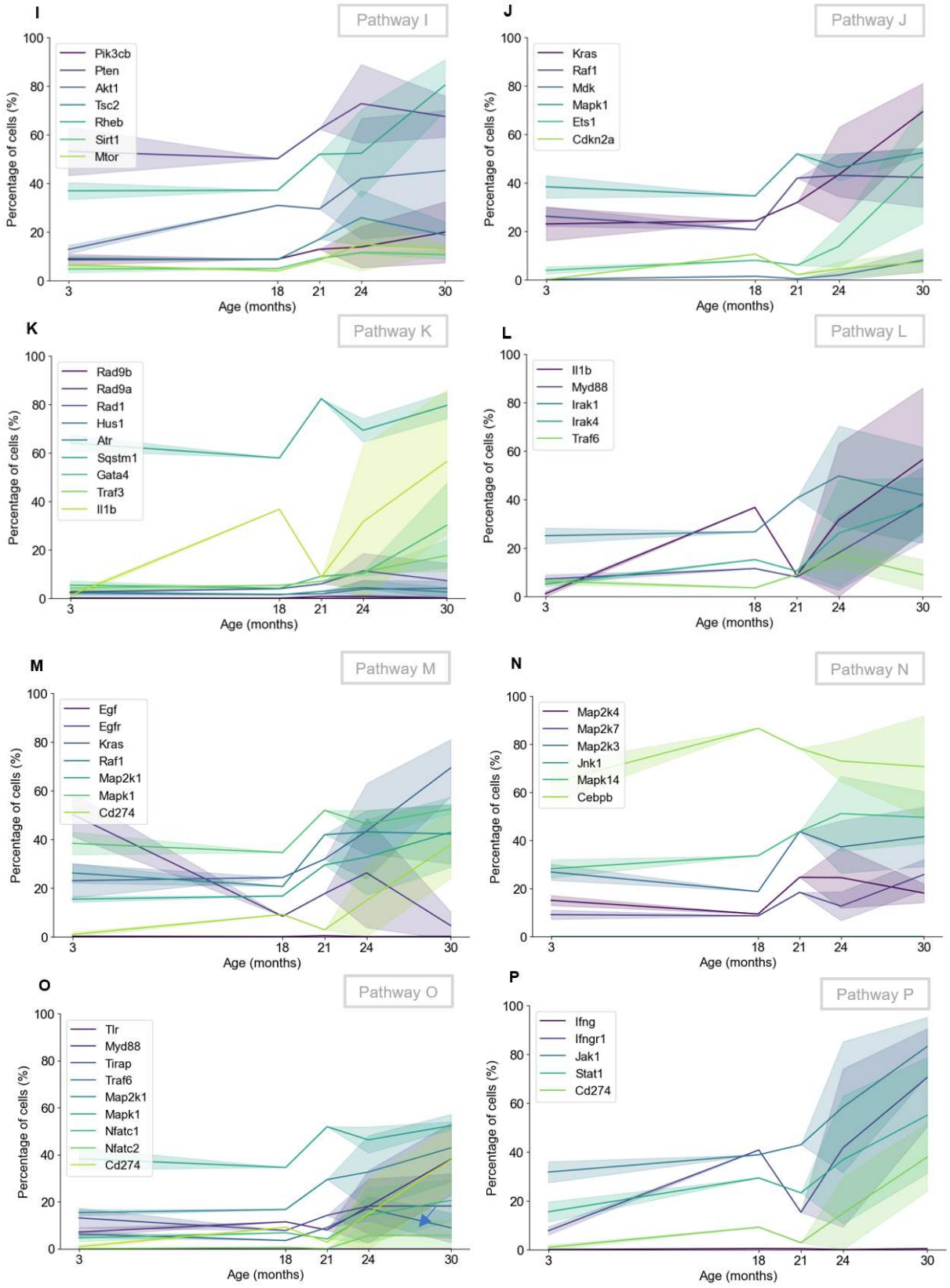

Supplementary figure 6. Pathway dynamics of pathways I-P. *Percentage of hepatocytes, Kupffer cells and endothelial cells expressing a gene per timepoint. The corresponding pathway maps are visualized in Supplementary figure 1-5.Conversion of gene names to protein names can be found in Supplementary table 1.*

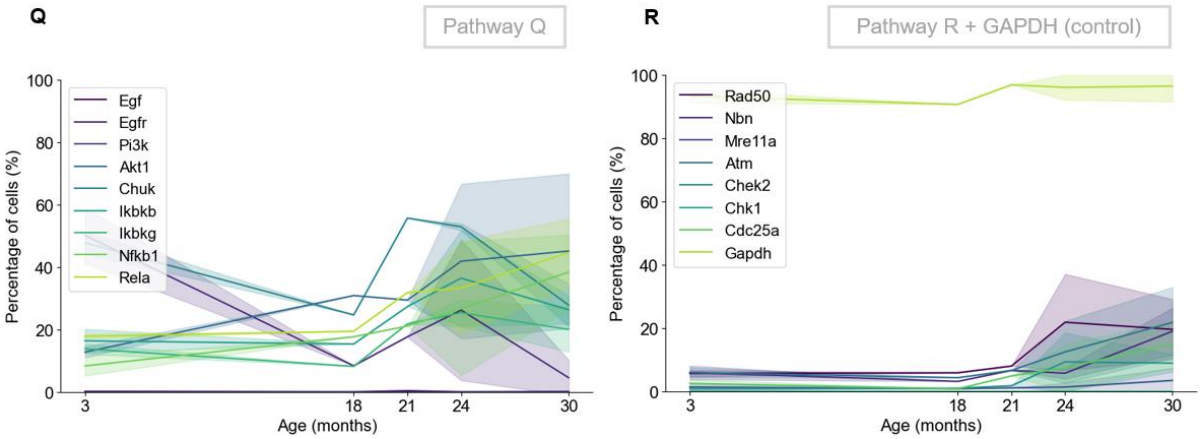

Supplementary figure 7. Pathway dynamics of pathways Q and R. *Percentage of hepatocytes, Kupffer cells and endothelial cells expressing a gene per timepoint. The corresponding pathway maps are visualized in Supplementary figure 1-5.Conversion of gene names to protein names can be found in Supplementary table 1.*

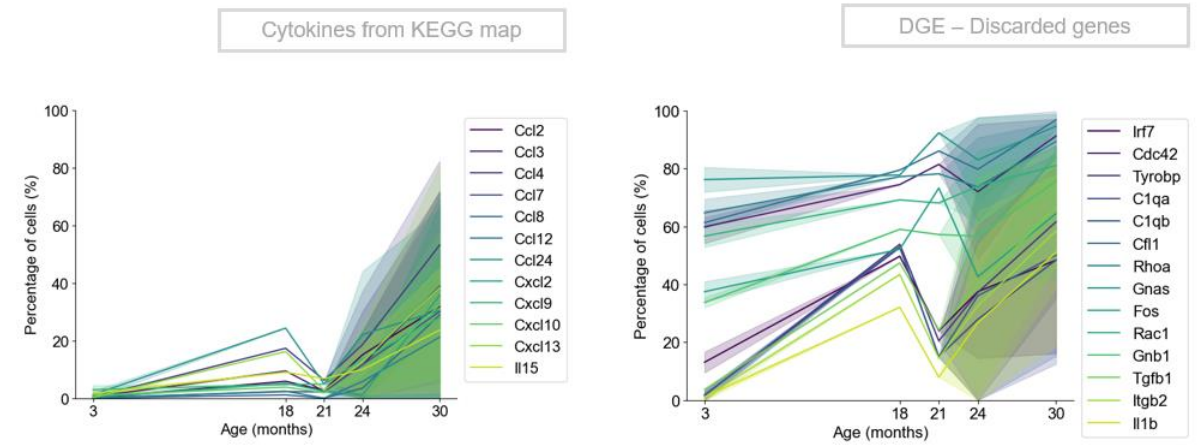

Supplementary figure 8. *Dynamics of the cytokines from all cytokines of the KEGG pathway maps with suitable dynamics (left). Dynamics of discarded genes from DGE (right).*

Equation 3. Model A.

$$\frac{dCCA}{dt} = k_{b\_cca} + k_{p\_cca} * CCA - k_{d\_cca} * CCA$$

$$\frac{dSASP}{dt} = k_{b\_sasp} + k_{p\_sasp\_cca} * CCA + k_{p\_sasp} * SASP - k_{d\_sasp} * SASP$$

Supplementary table 2. Fitted parameters for model A.

CCA	k_{b_cca}	k_{p_cca}	k_{d_cca}		sf_{cca}	$offset_{cca}$
	0.7416	0.4104	0.3190		0.2568	0.3255
SASP	k_{b_sasp}	$k_{p\_sasp\_cca}$	k_{p_sasp}	k_{d_sasp}	sf_{sasp}	$offset_{sasp}$
	0.6256	0.1461	0.9440	0.7537	0.008950	0.9803

Equation 4. Model B.

$$\frac{dCCA}{dt} = k_{b\_cca} + k_{p\_cca} * CCA - k_{d\_cca} * CCA$$

$$\frac{dSASP}{dt} = k_{b\_sasp} + k_{p\_sasp\_cca} * CCA + k_{p\_sasp} * SASP - k_{d\_sasp} * SASP$$

$$\frac{dSEN}{dt} = k_{b\_sen} + k_{p\_sen\_cca} * CCA + k_{p\_sen\_sasp} * SASP - k_{d\_sen} * SEN$$

Supplementary table 3. Fitted parameters for model B.

CCA	k_{b_cca}	k_{p_cca}	k_{d_cca}		sf_{cca}	$offset_{cca}$
	0.03105	0.3772	0.3260		1.188	1.727
SASP	k_{b_sasp}	$k_{p\_sasp\_cca}$	k_{p_sasp}	k_{d_sasp}	sf_{sasp}	$offset_{sasp}$
	0.4466	0.003844	0.1259	0.06876	0.6973	0.1663
SEN	k_{b_sen}	$k_{p\_sen\_cca}$	$k_{p\_sen\_sasp}$	k_{d_sen}	sf_{sen}	$offset_{sen}$
	0.7162	0.2123	0.2047	0.4562	1.433	0.4720

Equation 5. Model C.

$$\frac{dCCA}{dt} = k_{b\_cca} + k_{p\_cca} * CCA - k_{d\_cca} * CCA$$

$$\frac{dSASP}{dt} = k_{b\_sasp} + k_{p\_sasp\_cca} * CCA + k_{p\_sasp\_sen} * SEN + k_{p\_sasp} * SASP - k_{d\_sasp} * SASP$$

$$\frac{dSEN}{dt} = k_{b\_sen} + k_{p\_sen\_cca} * CCA + k_{p\_sen\_sasp} * SASP - k_{d\_sen} * SEN$$

Supplementary table 4. Fitted parameters for model C.

CCA	k_{b_cca}	k_{p_cca}	k_{d_cca}			sf_{cca}	$offset_{cca}$
	0.3464	0.05922	0.008481			1.031	3.085
SASP	k_{b_sasp}	$k_{p\_sasp\_cca}$	$k_{p\_sasp\_sen}$	k_{p_sasp}	k_{d_sasp}	sf_{sasp}	$offset_{sasp}$
	0.001569	0.008095	0.09544	0.07284	0.6767	0.1001	0.3473
SEN	k_{b_sen}	$k_{p\_sen\_cca}$	$k_{p\_sen\_sasp}$	k_{d_sen}		sf_{sen}	$offset_{sen}$
	0.8767	0.9121	0.09544	1.555		1.464	0.2565

Equation 6. Model D.

$$\frac{dCCA}{dt} = k_{b\_cca} + k_{p\_cca} * CCA - k_{d\_cca} * CCA$$

$$\frac{dSASP}{dt} = k_{b\_sasp} + k_{p\_sasp\_cca} * CCA + k_{p\_sasp\_sen} * SEN + k_{p\_sasp} * SASP - k_{d\_sasp} * SASP$$

$$\frac{dSEN}{dt} = k_{b\_sen} + k_{p\_sen\_cca} * CCA - k_{d\_sen} * SEN$$

Supplementary table 5. Fitted parameters for model D.

CCA	k_{b_cca}	k_{p_cca}	k_{d_cca}			sf_{cca}	$offset_{cca}$
	0.4813	0.5003	0.4564			1.143	2.520
SASP	k_{b_sasp}	$k_{p\_sasp\_cca}$	$k_{p\_sasp\_sen}$	k_{p_sasp}	k_{d_sasp}	sf_{sasp}	$offset_{sasp}$
	0.1454	0.5791	0.025539	0.07775	0.09594	9.331	0.3781
SEN	k_{b_sen}	$k_{p\_sen\_cca}$	k_{d_sen}			sf_{sen}	$offset_{sen}$
	0.6386	0.5791	0.6198			0.9192	5.356

Equation 7. Model E.

$$\frac{dACT}{dt} = k_{act} * ACT$$

$$\frac{dCCA}{dt} = k_{b\_cca} + k_{p\_cca} * CCA + k_{p\_cca\_act} * ACT - k_{d\_cca} * CCA$$

$$\frac{dSASP}{dt} = k_{b\_sasp} + k_{p\_sasp\_cca} * CCA + k_{p\_sasp\_sen} * SEN - k_{d\_sasp} * SASP$$

$$\frac{dSEN}{dt} = k_{b\_sen} + k_{p\_sen\_cca} * CCA - k_{d\_sen} * SEN$$

Supplementary table 6. Fitted parameters for model E.

ACT	ACT	k_{act}				
	0.4096	0.2043				
CCA	k_{b_cca}	k_{p_cca}	$k_{p\_cca\_act}$	k_{d_cca}	sf_{cca}	$offset_{cca}$
	0.1512			0.8361	0.8649	6.841
SASP	k_{b_sasp}	$k_{p\_sasp\_sen}$	$k_{p\_sasp\_cca}$	k_{d_sasp}	sf_{sasp}	$offset_{sasp}$
	0.4876	0.02240	0.1956	0.03784	0.2014	0.5316
SEN	k_{b_sen}	$k_{p\_sen\_cca}$	k_{d_sen}		sf_{sen}	$offset_{sen}$
	0.2032	0.7464	0.05293		1.0326	4.078

Equation 8. Model F.

$$\frac{dACT}{dt} = k_{act} * ACT$$

$$\frac{dCCA}{dt} = k_{b\_cca} + k_{p\_cca} * CCA + k_{p\_cca\_act} * ACT - k_{d\_cca} * CCA$$

$$\frac{dSASP}{dt} = k_{b\_sasp} + k_{p\_sasp\_cca} * CCA + k_{p\_sasp\_sen} * SEN + k_{p\_sasp} * SASP - k_{d\_sasp} * SASP$$

$$\frac{dSEN}{dt} = k_{b\_sen} + k_{p\_sen\_cca} * CCA - k_{d\_sen} * SEN$$

Supplementary table 7. Fitted parameters for model F.

ACT	ACT	k_{act}					
	0.4857	0.1635					
CCA	k_{b_cca}	k_{p_cca}	$k_{p\_cca\_act}$	k_{d_cca}		sf_{cca}	$offset_{cca}$
	0.8894	0.06154	1.752	0.6197		1.057	4.032
SASP	k_{b_sasp}	$k_{p\_sasp\_cca}$	$k_{p\_sasp\_sen}$	k_{p_sasp}	k_{d_sasp}	sf_{sasp}	$offset_{sasp}$
	0.7159	0.01690	0.008055	0.4210	0.3499	1.288	-0.006556
SEN	k_{b_sen}	$k_{p\_sen\_cca}$	k_{d_sen}			sf_{sen}	$offset_{sen}$
	0.7290	0.2991	0.2717			2.497	-9.626

Equation 9. Model G.

$$\frac{dCCA}{dt} = k_{b\_cca} + k_{p\_cca} * CCA - k_{d\_cca} * CCA$$

$$\frac{dSEN}{dt} = k_{b\_sen} + k_{p\_sen\_cca} * CCA - k_{d\_sen} * SEN$$

Supplementary table 8. Fitted parameters for model G.

CCA	k_{b_cca}	k_{p_cca}	k_{d_cca}	sf_{cca}	$offset_{cca}$
	0.1089	0.8100	0.7135	0.3473	0.7636
SEN	k_{b_sen}	$k_{p\_sen\_cca}$	k_{d_sen}	sf_{sen}	$offset_{sen}$
	0.7625	1.048	0.6197	0.2128	2.235

Equation 10. Model H.

$$\frac{dSASP}{dt} = k_{b\_sasp} + k_{p\_sasp} * SASP - k_{d\_sasp} * SASP$$

$$\frac{dSEN}{dt} = k_{b\_sen} + k_{p\_sen\_sasp} * SASP - k_{d\_sen} * SEN$$

Supplementary table 9. Fitted parameters for model H.

SASP	k_{b_sasp}	k_{p_sasp}	k_{d_sasp}	sf_{sasp}	$offset_{sasp}$
	0.5375	0.2825	0.2819	0.003941	0.3743
SEN	k_{b_sen}	$k_{p\_sen\_sasp}$	k_{d_sen}	sf_{sen}	$offset_{sen}$
	1.808	0.3268	0.07889	1.265	2.071

Supplementary table 10. Overview of the rules for the Boolean model.

Node	Rule for activation
Anti-inflammatory SASP (aSASP)	!(M1 & TL) & SC | RSC
Senescent cell (SC)	!TL | aSASP & !M1
Resistant senescent cell (RSC)	SC
Anti-inflammatory macrophage (M2)	aSASP
Pro-inflammatory macrophage (M1)	!RSC & SC
T lymphocyte (TL)	SC & !RSC& !M2

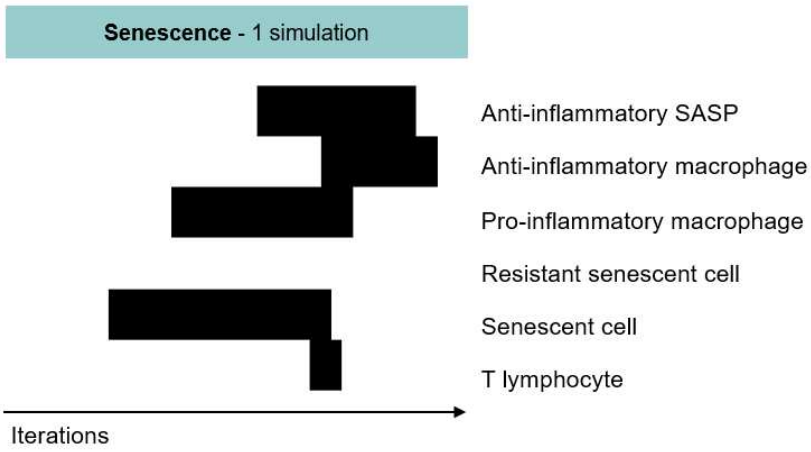

Supplementary figure 9. Scenario A - active senescent cell. *Only one simulation is shown. Black indicates the node is on, white indicates it is off.*